Remote Sensing of Environment 209 (2018) 660–676

Contents lists available at ScienceDirect

Remote Sensing of Environment

journal homepage: www.elsevier.com/locate/rse

Analyzing floating and bedfast lake ice regimes across Arctic Alaska using 25 years of space-borne SAR imagery

Melanie Engram[a,*], Christopher D. Arp[a], Benjamin M. Jones[b], Olaniyi A. Ajadi[c], Franz J. Meyer[c]

[a] Water and Environmental Research Center, University of Alaska Fairbanks, Fairbanks, AK, United States
[b] Alaska Science Center, U.S. Geological Survey, Anchorage, AK, United States
[c] Geophysical Institute, University of Alaska Fairbanks, Fairbanks, AK, United States

ARTICLE INFO

Keywords:
Arctic lakes
Ice regime
Lake ice
Overwinter fish habitat
Permafrost thaw
Synthetic aperture radar
Thermokarst lakes
Winter water supply

ABSTRACT

Late-winter lake ice regimes are controlled by water depth relative to maximum ice thickness (MIT). When MIT exceeds maximum water depth, lakes freeze to the bottom with bedfast ice (BI) and when MIT is less than maximum water depth lakes have floating ice (FI). Both airborne radar and space-borne synthetic aperture radar (SAR) imagery (Ku-, X-, C-, and L-band) have been used previously to determine whether lakes have a BI or FI regime in a given year, across a number of years, or across large regions. In this study, we use a combination of ERS-1/2, RADARSAT-2, Envisat, and Sentinel-1 SAR imagery for seven lake-rich regions in Arctic Alaska to analyze lake ice regime extents and dynamics over a 25-year period (1992–2016). Our interactive threshold classification method determines a unique statistic-based intensity threshold for each SAR scene, allowing for the comparison of classification results from C-band SAR data acquired with different polarizations and incidence angles. Additionally, our novel method accommodates declining signal strength in aging extended-mission satellite SAR instruments. Comparison of SAR ice regime classifications with extensive field measurements from six years yielded a 93% accuracy. Significant declines in BI regimes were only observed in the Fish Creek area with 3% of lakes exhibiting transitional ice regimes—lakes that switch from BI to FI during this 25-year period. This analysis suggests that the potential conversion from BI to FI regimes is primarily a function of lake depth distributions in addition to regional differences in climate variability. Remote sensing of lake ice regimes with C-band SAR is a useful tool to monitor the associated thermal impacts on permafrost, since lake ice regimes can be used as a proxy for of sub-lake permafrost thaw, considered by the Global Climate Observing System as an Essential Climate Variable (ECV). Continued winter warming and variable snow conditions in the Arctic are expected and our long-term analysis provides a valuable baseline for predicting where potential future lake ice regimes shifts will be most pronounced.

1. Introduction

Shallow lakes are abundant in many regions of the Arctic, primarily due to prior glaciation and degradation of near surface ice-rich permafrost (Duguay et al., 2003; Grosse et al., 2013; Smith et al., 2007). Traditionally, winter lake ice grows 1.5 to 2 m thick at maximum ice thickness (MIT) and shallow lakes with depths less than MIT freeze completely and are called bedfast ice (BI) lakes (Brewer, 1958; Sellmann et al., 1975). Lakes with depths greater than MIT retain some liquid water and are termed floating ice (FI) lakes (Jeffries et al., 1996). Differences between BI and FI regimes in thermokarst lakes (see Appendix 1 for a glossary of abbreviations) are important because lakes with an above freezing (> 0 °C) mean annual bottom temperature will cause sub-lake permafrost degradation (Arp et al., 2016; Brewer, 1958; Burn, 2002). Additionally, BI and FI conditions impact energy and water balance (Arp et al., 2015). In regions where most lakes have BI regimes, lakes with FI provide often limit overwintering fish habitat and winter water supply for ice road construction and municipal uses (Jones et al., 2009). Yet despite this key dichotomy between arctic lakes, relatively little is known about several key features of these lakes: a) the distribution of lakes by ice regime over large regions, b) how regional lake ice regimes vary over time, and c) how they may be changing in response to climate change.

Landscape-scale inventories of lake ice regimes were first made by recognizing that BI lakes consistently become ice-free earlier than adjacent FI lakes due in part to thinner ice (Brewer, 1958) but also due to inability of surface melt-water to drain from ice-cover in BI lakes in comparison to FI lakes (Arp et al., 2015). Sellmann et al. (1975) used

* Corresponding author at: Water and Environmental Research Center, 306 Tanana Loop, P.O. Box 5860, Fairbanks, AK 99775-5860, United States.
E-mail address: melanie.engram@alaska.edu (M. Engram).

https://doi.org/10.1016/j.rse.2018.02.022
Received 29 August 2017; Received in revised form 8 February 2018; Accepted 15 February 2018
Available online 19 March 2018

early summer Landsat imagery across portions of the Arctic Coastal Plain of northern Alaska to distinguish between relatively shallow lakes (BI) and relatively deep lakes (FI). Early uses of side-looking airborne radar (SLAR) showed a marked difference in the radar return from FI (high backscatter) and BI (low backscatter) lakes on Alaska's North Slope (Weeks et al., 1977). This sharp separation between backscatter from BI and FI was attributed to the large difference in dielectric properties between ice and fresh water along with the presence of small tubular bubbles in the ice (Mellor, 1982; Weeks et al., 1978, 1981). Field measurements revealed that while a uniform area of high backscatter indicated FI, low backscatter could indicate BI or the presence of briney water remaining under the ice cover at MIT (Mellor, 1982). Additionally, an ambiguous low radar signal was returned from FI on lakes deeper than ~4 m, which was attributed to the absence of tubular dissolved gas bubbles in ice over deep water (Mellor, 1982).

With the advent of calibrated space-borne synthetic aperture radar (SAR), Jeffries et al. (1994) and Morris et al. (1995) quantified the high and low backscatter intensity (σ^0) from FI and BI lakes, attributing the high σ^0 from FI lakes to the high dielectric contrast at the ice/water interface along with the presence of tubular gas bubbles, and low σ^0 from BI lakes to the low dielectric contrast at the ice/soil interface. They conducted field research at the same locations as the geocoded SAR pixels, establishing C-band SAR with a vertical transmit and receive (VV) single polarization as a useful remote sensing tool for landscape-scale lake regime inventory. Duguay et al. (2002) examined the effect of imaging incidence angle on horizontal transmit and receive (HH) C-band SAR-based ice regime analysis. Jones et al. (2013) successfully used X-band SAR to distinguish between BI and FI lake, river, and beaded stream ice regimes in northern Alaska, while Gunn et al. (2015) used X-band and the even shorter Ku-band on lake ice in Manitoba, Canada. Engram et al. (2013) evaluated L-band single and quadrature polarized backscatter from FI and BI as inferior to C-band VV σ^0 for distinguishing between the two regimes. Investigators have used SAR data to determine winter water availability from FI lakes for use in oil exploration (French et al., 2004; Jeffries et al., 1996; White et al., 2008). Others emphasized lake ice regime information from SAR in the context of climate research (Hall et al., 1994; Morris et al., 1995) and habitat studies (Brown et al., 2010; Jones et al., 2013). Recent investigations using polarimetric C-band SAR data by Atwood et al. (2015) have clarified the specific scattering mechanism that causes high σ^0 from FI. SAR is an established remote sensing tool to determine contrasting lake ice regimes, and a concise summary of various SAR imaging parameters and list of lake ice classification studies appears in Duguay et al. (2015). SAR's ability to image at night and through dry snow to provide landscape-scale lake ice regime classifications makes it a valuable tool for mapping lake ice regimes in the often cloudy and dark Arctic.

Late winter lake ice regimes are known to vary from year to year within and between regions (Arp et al., 2012; Duguay et al., 2002; Jeffries et al., 1994; Surdu et al., 2014). MIT variability can be related to differences in winter temperatures as well as the amount and timing of snowfall (Zhang and Jeffries, 2000). These differences in winter climate along with fluctuations in water level during the open-water period can cause lakes to transition from one ice regime to another in a given year. A shift from BI to FI could indicate thinner lake ice, or it could indicate an increase in lake water balance. A shift from FI to BI could indicate thicker ice, or it could be the result of a decrease in lake water balance (Arp et al., 2012). Deciphering causes of shifting ice regimes or ice regime variability requires consideration of both regional lake depth distributions and changes in climate that affect lake ice and water balance, although lake-specific variation such as partial lake drainage needs to be considered as well (Jones et al., 2009). Thus, analyzing a time series of SAR data at the regional scale is important for better understanding the impact of climate change on BI and FI regimes in arctic lakes.

In addition to examining lake ice regime change as a response to climate change, we can also map lake ice regimes using SAR to indicate the extent of permafrost thaw beneath lakes across the Arctic landscape. Lakes and permafrost have both been identified as Essential Climate Variables (ESVs) by the Global Climate Observing System (Bojinski et al., 2014). Although there are no direct remote sensing methods to detect and measure permafrost (Trofaier et al., 2017), lake ice regimes provide a proxy to the state of the permafrost below thermokarst lakes: liquid water under lake ice at MIT provides a thermal environment above the freezing point all winter, preventing re-freezing of the active layer in sub-lake permafrost, and promoting talik (thaw bulb) development.

Recent studies have broken ground in using SAR to develop landscape-scale inventories of lake ice regimes but have focused on one region for a 20-year timespan (Surdu et al., 2014), or a larger geographic area, such as the North Slope Alaska (Grunblatt and Atwood, 2014) and the pan-Arctic (Bartsch et al., 2017) based on one year. In this study, we analyze 25 years of space-borne C-Band SAR data acquired from multiple platforms covering seven lake-rich study regions in Arctic Alaska. Our study involves 11,571 lakes located in 15,250 km^2 of Arctic tundra landscape. The seven study sites differ in terms of climate and physiography, but are all located in the continuous permafrost zone in Alaska.

Our novel classification methodology allowed us to determine BI and FI across several C-Band SAR platforms to determine regional responses in ice regimes between 1992 and 2016. Our SAR-based classification quantitatively shows the amount of lake-scape area that is affected by variations in ice regimes from year to year, as well as the number and area of lakes that are predominantly BI, FI, or display intermittent ice regimes (INT) that oscillate between regimes, or have transitioned from BI to FI (TRANS-FI) or FI to BI (TRANS-BI) over this 25-year period. Our analysis identifies the composition of lake ice regimes across different lake-rich arctic landscapes and their susceptibility to future change, providing valuable remote sensing information about permafrost and lakes, both of which have been identified as ECVs.

2. Methods

2.1. Study area

To investigate patterns and any trends over the last 25 years that may be occurring in lake ice regimes, we chose seven regions in Alaska: five lake regions in the Arctic Coastal Plain of northern Alaska (ACPnA), one in the North Slope foothills, and one on the northern Seward Peninsula to represent a variety of thermokarst lake types including coastal and inland sites, high and low ice content in permafrost, and a variety of soil types (Fig. 1). Regions were selected based on representation of known lake, physiographic, and climatic variation in Arctic Alaska, but are not watershed based. Regions represent different limnologic landscapes that are all fairly lake-rich, but have different surface geologies that factor into lake depth, snow distribution, and water balance, which in turn affect lake ice regimes. Ground ice content varies between regions, as does surface geology, elevation, and topography.

Several years of measurements from field campaigns and from literature exist for many lakes in the regions near Barrow, Teshekpuk, Fish Creek, Inigok, Umiat and northern Seward Peninsula (Table 1), while lakes in the lower Kuparuk River region are possible subjects of future field investigations. Additionally, very few of the lakes in these areas are accessible by road, which reduces the risk of sampling bias due to easy access. Exact domains of each region were delineated to capture similar lake characteristics and at sizes of comparable magnitude (11,000–35,000 km^2). The percentage of lake-covered area within the regions is variable, ranging from 1% to 26% and the number of lakes per region varies from 123 to 2548 lakes (Table 2).

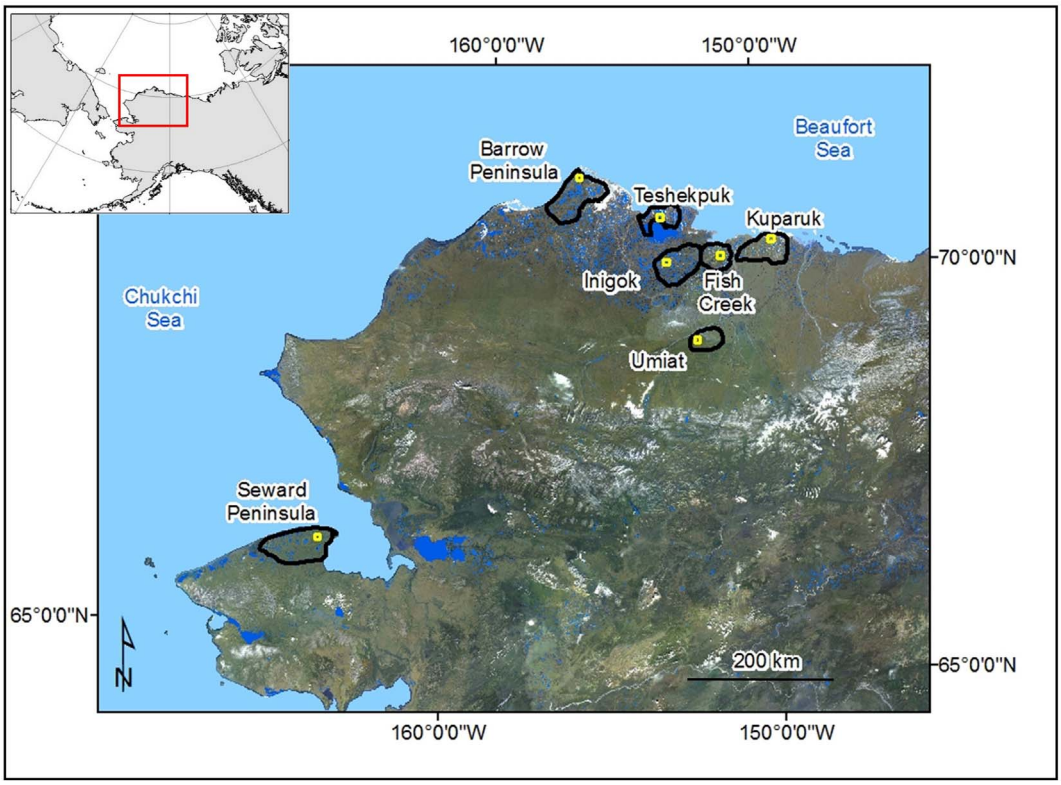

Fig. 1. Seven study areas in the continuous permafrost region outlined in black, from the north, clockwise: Barrow Peninsula, Teshekpuk Lake Special Area, Inigok, Fish Creek, Kuparuk, Umiat, and Northern Seward Peninsula (NSP). Yellow outlines indicate spatial extents featured in Figs. 6 through 13. Background image is SPOT false color RGB from Geographic Information Network of Alaska. Lakes are highlighted in blue from the Global Wetlands Database (Lehner and Döll, 2004). Background image is Best Data Layer from http://gis.dnr.alaska.gov/.

2.2. SAR imagery and scene selection

Scenes were selected to capture MIT, which typically occurs in April, but before the onset of spring melt, which typically occurs in mid-May, to avoid dampening the SAR signal from the presence of water on the ice surface. Where April scenes were not available, we used images from late March or early May (Table 3). We used C-band SAR (wavelength = 5.6 cm), which has been shown to provide the best contrast between BI and FI (Engram et al., 2013). We checked local meteorological data for air temperature to make sure data were not acquired during a warm-snap (Grunblatt and Atwood, 2014).

We compiled late winter SAR scenes from six different C-band SAR space-borne platforms (Table 3) to create the longest ice regime classification timeline with near-annual temporal resolution, to our knowledge, yet reported. No single space-borne SAR instrument was in operation for these 25 years, therefore our methods necessitated cross-platform continuity as well as accounting for single-platform instrument power loss between years. From 1992 through 2011, we used ERS-1 and ERS-2 data which were acquired with a VV polarization and an incidence angle of ~23°. During this time-window, data gaps were filled with RADARSAT-1 Standard Beam 5 data, acquired in HH polarization and ~37°–42° incidence angle. Data from both platforms were calibrated and geocoded to a pixel size of 12.5 m. For 2011–2012, we used Envisat ASAR Wide Beam (HH, 15°–42° incidence angle) which was geocoded to a 75 m pixel size. From 2013 to 2014, we acquired RADARSAT-2 ScanSAR-A (HH, 20°–49° incidence angle) with pixel size of 50 m. For 2015–2016, we used Sentinel-1: for 2015 we used Interferometric Wide Swath with dual polarization (VV and VH, ~38° incidence angle) with 10 m pixel size, and for 2016 we used Extra Wide Swath (HH and HV, ~35° incidence angle) with 40 m pixel size.

2.3. SAR data processing methods

All ERS-1, ERS-2, and RADARSAT-1 were available as Single Look Complex (SLC) images through the services of the Alaska Satellite Facility (ASF). All data were first radiometrically calibrated using

Table 1
Ten-year record of maximum lake ice thickness for each region in this study (all measurements made from multiple lakes between early March to early May and standardized to maximum thickness value based on fitting observed thickness to ice growth curve using local weather station air temperature data applied to the modified Stefan equation). Full dataset and metadata are available at: https://doi.org/10.18739/A2G27V.

	Annual maximum ice thickness (cm)									
Region	2007	2008	2009	2010	2011	2012	2013	2014	2015	2016
Barrow	175	153	151	161	174	177	177	126	145	181
Teshekpuk	178	168	147	165	137	174	169	142	157	177
Fish Creek	144	135	131	164	125	148	183	141	176	174
Kuparuk	–	–	–	–	–	–	–	–	–	–
Inigok	–	–	–	–	130	148	179	138	165	141
Umiat	–	–	–	–	–	114	150	127	104	91
Seward Peninsula	96	107	121	144	121	–	–	–	–	–

Table 2
Lake regions were selected to represent a variety of surface geologies, lake densities, permafrost depths, and ground ice volume.

Region	Landscape	Surface geology[b]	N lakes	Area of Region (km^2)	Percentage of landscape covered by lakes	Permafrost depth (m)	Ground ice volume[b]
Barrow	Outer and Younger Outer ACP[a]	Alluvial-Marine, Glaciomarine	2228	3067	23%	200–410[b]	Moderate-High
Teshekpuk	Younger Outer ACP[a]	Glaciomarine	697	1696	16%	370[b]	High
Fish Creek	Inner ACP[a]	Eolian: sand, Alluvial-Marine	1331	1265	15%	220[b]	Low-Moderate
Kuparuk	Younger Outer ACP[a]	Alluvial-Marine	2548	2109	12%	[c]	Moderate
Inigok	Inner ACP[a]	Eolian: sand	2302	2461	26%	290[b]	Low
Umiat	Foothills	Eolian: loess (yedoma), Colluvial: hillside	123	1099	1%	240[b]	Moderate-High
Seward Peninsula	Coastal	Eolian: loess (yedoma)	2350	3553	7%	> 90[d]	High

[a] From Hinkel et al., 2005.
[b] From Jorgenson et al., 2008.
[c] No permafrost depth listed in dataset.
[d] Hopkins (1949), Hopkins et al. (1955).

published calibration factors and then geocoded to arrive at sigma-naught-scaled terrain-corrected geotiff files. Geocoding was done using the MapReady software (v3.1.24) as well as elevation data from the IfSAR DTM derived from data acquired in 2002–2006 and 2012. SLC data from Envisat single polarization Wide Swath, RADARSAT-2 ScanSAR Wide A, and Sentinel-1 were calibrated to sigma-naught and terrain-corrected using the Sentinel Application Platform (SNAP) tool suite provided by ESA. The Global Earth Topography And Sea Surface Elevation at 30 arc-second resolution (GETASSE30) elevation dataset was used to geocode these data. We applied a Lee Sigma speckle filter (Lee, 1981) in ERDAS Imagine (v2014), then manually checked and refined the geolocation accuracy of each image using a lateral translation. We mosaicked SAR scenes in three cases for the NSP region using the ERSI ArcMap software (v10.3) where data were only available in orbits providing partial coverage (Table 3, italics), choosing scenes at MIT as close to each other as possible. Due to near-log normal characteristics of power-scaled SAR data (Dekker, 1998), we performed a log-transform on the filtered radar intensity values resulting in data that were near-Gaussian distributed. Envisat ASAR data were provided by the European Space Agency, and RADARSAT-2 data was purchased from McDonald Detweiller Association.

Lake perimeters for each region were derived from IfSAR elevation data including use of Western Arctic Coastal Plain lake perimeters (Jones and Grosse, 2013). To account for the expansion of thermokarst lakes that occurred between the early 1990's and the early 2000's, we manually retro-fitted some rapidly expanding lake perimeters in the Teshekpuk region using 1992 Landsat imagery. This correction insured the exclusion of bright land pixels along expanding shorelines in the

Table 3
SAR acquisition dates and imaging parameters, including platform, polarization, nominal incidence angle at scene center, and pixel size. Data frames were selected to cover each region entirely, often necessitating selection of different orbits for adjacent regions.

Year	Barrow	Fish Creek	Inigok	Kuparuk	Seward Peninsula	Teshekpuk	Umiat
1992	20-Apr[a]	24-Apr[a]	27-Apr[a]	21-Apr[a]	*26-Apr*, *26-Apr*[a]	14-Apr[a]	24-Apr[a]
1993	21-Apr[a]	28-Apr[a]	1-May[a]	25-Apr[a]	30-Apr[a]	15-Apr[a]	25-Apr[a]
1994	29-Apr[a]	21-Apr[a]	21-Apr[a]	27-Apr[a]	20-Apr[a]	22-Apr[a]	24-Apr[a]
1995	14-Apr[a]	21-Apr[a]	21-Apr[a]	18-Apr[a]	23-Apr[a]	8-Apr[a]	18-Apr[a]
1996	3-May[a]	3-Apr[a]	23-Mar[a]	19-Apr[b]	*22-Mar*, *4-Apr*[a]	–	1-Mar[b]
1997	19-Apr[b]	24-Apr[b]	–	21-Apr[b]	21-Mar[b]	13-Apr[b]	12-Apr[b]
1998	23-Apr[b]	28-Apr[b]	30-Apr[b]	24-Apr[b]	13-Apr[b]	14-Apr[b]	8-Apr[b]
1999	24-Apr[b]	–	30-Apr[b]	22-Apr[c]	30-Apr[b]	18-Apr[b]	12-Apr[b]
2000	8-Apr[b]	1-May[b]	18-Apr[b]	29-Apr[b]	*29-Mar*, *1-Apr*[b]	16-Apr[b]	1-May[b]
2001	28-Apr[b]	13-Apr[b]	20-Apr[b]	29-Apr[b]	–	22-Apr[b]	20-Apr[b]
2002	2-May[b]	18-Apr[b]	5-Apr[b]	14-Apr[b]	*3-Apr*[b]	26-Apr[b]	5-Apr[b]
2003	17-Apr[b]	21-Apr[b]	24-Apr[b]	18-Apr[b]	19-Mar[b]	27-Apr[b]	21-Apr[b]
2004	6-May[b]	24-Apr[b]	27-Apr[b]	22-Apr[b]	22-Mar[b]	9-Apr[b]	25-Apr[b]
2005	21-Apr[b]	25-Apr[b]	29-Apr[b]	22-Apr[b]	8-Apr[b]	29-Apr[b]	30-Apr[b]
2006	22-Apr[b]	27-Apr[b]	30-Apr[b]	8-Apr[b]	28-Apr[b]	30-Apr[b]	30-Apr[b]
2007	26-Apr[b]	15-Apr[b]	15-Apr[b]	27-Apr[b]	16-Apr[b]	20-Apr[b]	15-Apr[b]
2008	10-Apr[b]	1-May[b]	17-Apr[b]	30-Apr[b]	31-Mar[b]	20-Apr[b]	30-Apr[b]
2009	9-Apr[b]	19-Apr[b]	21-Apr[b]	13-Apr[b]	17-Apr[b]	24-Apr[b]	19-Apr[b]
2010	29-Apr[b]	20-Apr[b]	23-Apr[b]	16-Apr[b]	5-Apr[b]	23-Apr[b]	23-Apr[b]
2011	16-Apr[b]	25-Apr[d]	25-Apr[d]	29-Apr[b]	–	25-Apr[d]	–
2012	05-Apr[d]	05-Apr[d]	05-Apr[d]	05-Apr[d]	–	05-Apr[d]	–
2013	25-Apr[e]	25-Apr[e]	25-Apr[e]	25-Apr[e]	–	25-Apr[e]	–
2014	20-Apr[e]	20-Apr[e]	20-Apr[e]	20-Apr[e]	–	20-Apr[e]	–
2015	20-Apr[f]	22-Apr[f]	20-Apr[f]	22-Apr[f]	–	20-Apr[f]	22-Apr[f]
2016	12-Apr[g]	–	12-Apr[g]	–	–	12-Apr[g]	–

Italic indicates mosaic.
[a] ERS-1: VV, center θ ≈ 23°, pixel size = 12.5 m.
[b] ERS-2: VV, center θ ≈ 23°, pixel size = 12.5 m.
[c] RADARSAT-1 std. 5: HH, center θ ≈ 39°, pixel size = 12.5 m.
[d] Envisat HH, center θ ≈ 30°, pixel size = 75 m.
[e] RADARSAT-2 ScanSAR Wide A: HH, center θ ≈ 35°, pixel size = 50 m.
[f] Sentinel 1A IW: Interferometric Wide Swath (Level 1 product): VV and VH, center θ ≈ 33°, pixel size = 10 m.
[g] Sentinel 1A EW: Extra Wide Swath (Level 1 product): HH and HV, center θ ≈ 33°, pixel size = 40 m.

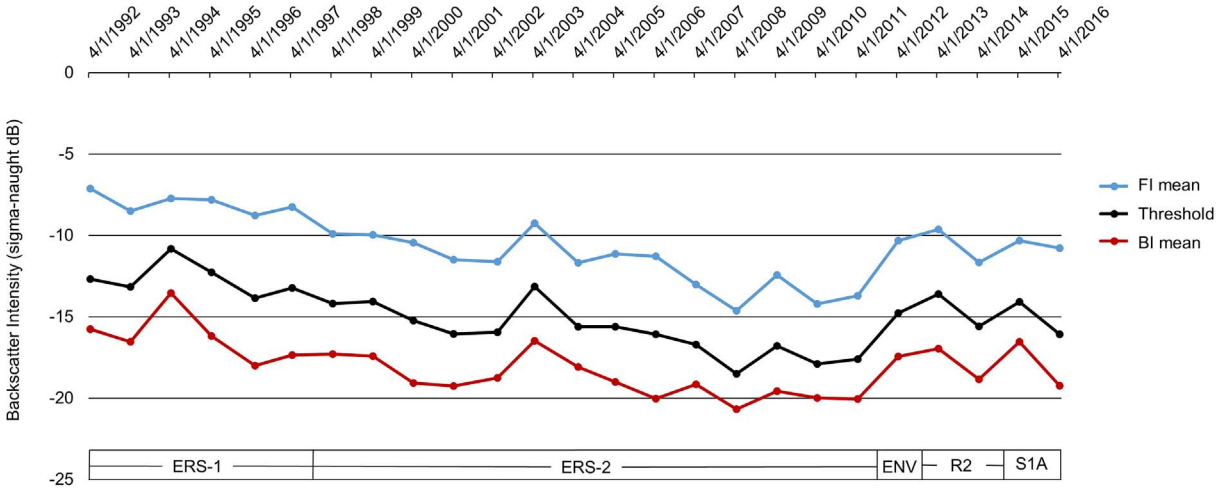

Fig. 2. Threshold, floating ice (FI) mean, and bedfast ice (BI) mean as derived from each SAR scene for the Barrow Peninsula region over the 25-year study period. Variances between years and SAR instruments necessitate determining a unique threshold for ice regimes from each SAR scene. ERS-1 was used between 1992 and 1996, ERS-2 used between 1997 and 2011, ENV denotes Envisat ASAR used for 2012, R2 denotes RADARSAT-2 used between 2013 and 2014, S1A denotes Sentinel 1A used for 2015 and 2016.

early 1990's when the lakes were smaller. The five Espenberg maars (large, deep lakes several kilometers in diameter) were excluded from this study, since they never freeze to lake bed. They are not thermokarst lakes, but a rare lacustrine phenomenon, thought to originate from violent phreato-permafrost-magmatic explosions (Hopkins, 1988) in which hot lava vaporizes water beneath a layer of permafrost.

2.4. Automatic and adaptive lake ice regime classification

In order to differentiate BI and FI, we used a threshold method on log-transformed SAR data (decibels) similar to previously published methods (Brown et al., 2010; French et al., 2004; Grunblatt and Atwood, 2014; Kozlenko and Jeffries, 2000). However, since we planned to use a variety of SAR platforms and since SAR instruments experience strength degradation over time, especially when operated past planned life design (Fig. 2), we could not use a single fixed threshold as did these previous studies. In order to account for changes in signal strength from identical instruments over time, changes in ice conditions, and changes in SAR imaging parameters from different instruments, we statistically determined the numeric value of the SAR threshold from the sigma-naught (σ^0) probability density function (PDF) of lake-ice pixels in each scene in the following manner. First, to remove residual speckle noise that remained after the application of the previously mentioned Lee Sigma filter, we utilized modern non-local filtering methods to effectively suppress noise while preserving most relevant image details. Non-local means filters are ideally suited for this task as they identify similar image patches in a dataset and use those patches to optimally suppress noise without sacrificing image resolution (Ajadi et al., 2016; Darbon et al., 2008). Next, lake ice pixels were selected from the SAR scene using a lake perimeter/land mask. Calibrated SAR backscatter information in σ^0 in dB scale from lake ice on all lakes in a scene displayed the combined PDF of darker BI ice and brighter FI regions, resulting in a joint PDF of bimodal character (Fig. 3).

From the bi-modal frequency distribution of the lake ice pixels for each filtered and log-transformed image, we utilized statistical data processing to determine an equal-error, unbiased threshold to classify lake ice pixels into two classes, namely FI pixels and BI pixels (Fig. 3). In estimating the unbiased threshold, the joint PDF was assumed to be composed of a mixture of two Gaussian distributions, one representing BI pixel and one containing FI data points (Ajadi et al., 2016; Dekker, 1998). To automate the identification of the parameters of these Gaussian distributions, we used an Expectation-Maximization (EM) approach. According to Ajadi et al. (2016), EM algorithms find the best

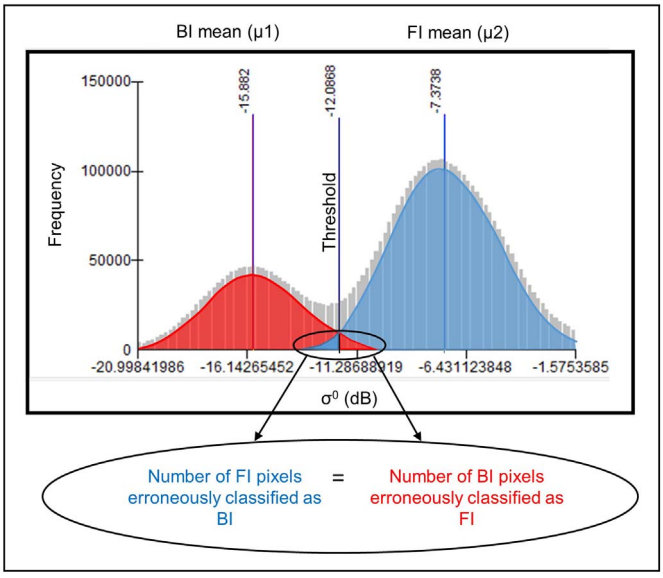

Fig. 3. Bimodal (mixed) frequency distribution of ERS-1 backscatter from lake ice indicating the means of BI and FI distributions with the overlap of bright BI pixels and dim FI pixels. SAR image acquisition date is April 15, 1993 from lakes in the Teshekpuk Lake Special Area. The percent of observations that are erroneously classified varies from scene to scene and is dependent upon the separation of the two means and their standard deviations. The threshold of −12.0868 dB was selected according to Eq. (1), in order that classification errors are equal in area across the landscape with no bias toward FI or BI.

fitting mixture of Gaussian distributions by following an iterative two-step procedure including an expectation step followed by a maximization step. Every pixel is assigned to the class with the highest probability, and a threshold value is estimated (Ajadi et al., 2016; Mercier and Girard-Ardhuin, 2006). Since the two frequency distributions of BI and FI pixels overlap, errors of misclassifying bright BI pixels as FI and misclassifying dim FI pixels as BI are unavoidable, but our method sets the estimated threshold at the point where there is an equal number of pixels with false-positive errors (Type 1) and errors of omission (Type 2) (Fig. 3). It is statistically unlikely that Type 1 or 2 errors outweighs one another using this method across the landscape, per Eq. (1), where $\mu 1$ and $\mu 2$ are BI and FI means respectively, *std*1 and *std*2 are standard deviations:

$$\text{Threshold} = \mu 1 + \left[\frac{\mu 2 - \mu 1}{(std1 + std2)} * std1 \right] \quad (1)$$

The outputs of the EM algorithm are the means and variances of SAR σ^0 for the two lake ice classes (BI and FI) as well as a threshold to divide them for each SAR scene. All algorithm outputs were manually checked against the frequency distributions of SAR lake ice pixels for each scene for goodness of fit evaluation, as is exhibited in Fig. 3. In the case of mosaicked scenes, cases were processed for each scene and again for the combined mosaic and the threshold that best fit the histogram of the mosaicked data was selected.

In regions where lakes predominantly exhibited a single ice regime (mostly FI or mostly BI), we used larger areal extents of lakes as input for threshold derivation in order to acquire a sufficiently large sample from both FI and BI populations. In areas of sparse lake density, we used a subset of the landscape showing high lake density since high lake density input to the threshold algorithm provided the most accurate results. In the northern Seward Peninsula for the years 1998 and 1999, the threshold algorithm failed to produce reasonable BI/FI means and thresholds, possibly due to a complication of low lake density in this region. We therefore interpolated means and thresholds for these years from those values of the previous and following full scenes (years 1996 and 2000) and checked the interpolated values for goodness of fit with the PDF of 1998 and 1999 lake ice pixels.

Lake ice pixels with a higher σ^0 than our determined threshold for that scene (which ranged from −9 to −19 dB) were classified as FI, those with a lower σ^0 were classified as BI. The advantages of deriving a unique threshold for each SAR scene rather than using a single threshold value for all years are 1) circumventing errors caused by decreasing instrument strength over time, 2) avoiding errors caused by variations in ice/bubbles/humidity and other undetermined factors that can cause variations in σ^0 values from BI and FI from day to day, and 3) allowing comparison of classification results from scenes using different C-band SAR imaging parameters, thus eliminating the need for incidence angle normalization. These methods thereby allowed for the development of a 25-year SAR-based time series of lake ice regimes.

2.5. Determining area of FI ice, number of lakes with each regime, and prevailing ice regime

Calculation of 1) the areal percentage of BI and FI ice and 2) the classification of each lake's ice regime were performed in ArcMap, using standard geoprocessing tools that we automated with Python scripting. For each year, we calculated the percentage of lake ice across the landscape that was either BI and FI using our novel no-bias threshold method described above, then summed the FI area from all lakes to calculate a regional FI percentage for that year.

We then considered the BI and FI pixels on each individual lake to determine a whole-lake classification for each year: a lake was considered to be a BI lake for that year if it had < 5% FI pixels per Arp et al. (2012). We classified FI lakes if they had at least 5% FI pixels and fulfilled the additional criterion of having 0.5% of pixel values higher than the FI mean. This additional requirement was added ad hoc to preclude false classification of large BI tundra lakes exhibiting high σ^0 from surface pressure ridges, appearing as bright linear features in the ice. Additional quality control of the lake ice regime classifications was conducted in a GIS environment. Common sources of error for individual lake regime classifications included geolocation errors where the lake image was offset from the lake perimeter, usually in higher-relief regions, and cracks in the ice of large lakes which caused false FI classification in the coastal regions in two of the years. Another source of error occurred when using larger pixels (40–75 m size) in the classification of small lakes (< 10 ha). Larger pixels used for years 2011–2014 and 2016 were often mixed pixels containing averaged σ^0 from FI and BI which resulted in false BI classifications for small lakes. These classification errors caused by poor geolocation, two years with surface artifacts in coastal regions, and large pixel size were obvious to the human eye and could be manually corrected in ArcMap (v10.3) by targeting 1) all lakes in the high-relief Umiat region and lakes in areas with known geolocation error, 2) small lakes in years with large pixels, 3) FI classification in the two years with pronounced cracks/surface ridges, We did not check every lake for every year, but at least 10% of lakes for all years were manually checked in ArcMap using temporal queries; for example, checking lakes that showed a single case of FI with a BI classification in all other years. We systematically checked every lake for all years that was FI < 90% of the time or BI < 90% of the time.

Examining the time series of lake ice regimes for each lake, we further classified each lake's ice regime history as one of five types: 1) Stable BI, 2) Stable FI, 3) TRANS-FI if it showed a trend over time of transitioning from BI to FI, 4) TRANS-BI if it showed a trend in time of transitioning from FI to BI, or 5) intermittent (INT). A lake was classified as Stable BI if it was classified as BI for 90% of the years or more, Stable FI if it had been classified as FI for 90% of the years or more, transitional if it showed a significant trend ($p \leq 0.05$) over the span of the SAR analysis from BI to FI (TRANS-FI) or from FI to BI (TRANS-BI), and INT if the lake oscillated between BI and FI regimes but showed no significant trend over time. For each region, we tested the annual FI area as well as the number of FI lakes for statistically significant trends over time. These time-series and all other statistical analyses were conducted in SPSS statistical software (v.22). Full dataset showing results from this analysis is archived at the National Science Foundation's Arctic Data Center (Engram, 2018).

2.6. Multi-sensor SAR validation

Due to our interactive threshold selection (Fig. 3), we were able to compile and compare the results of SAR analysis from seven different space-borne SAR platforms (Table 3), thereby creating the longest near-annual ice regime time-series record to date. These are all C-band SAR instruments, but use different polarizations and incidence angles while imaging. For this study, we used data that was acquired with both VV and HH polarizations and with incidence angles ranging from 21° to 44° over our study regions. To test whether our interactive threshold selection method accurately provided continuity across these SAR platforms, we compared classification results from SAR scenes acquired on the same day but with different polarizations and incidence angles (Table 4). For control, we compared an ERS-1 and ERS-2 scene acquired a day apart (same day passes were not available over our regions) to test variability that could be caused by geolocation errors or any other factors. To test the effect of different polarizations on SAR-based lake ice regime classification, we compared an ERS-2 SAR scene acquired using VV polarization with RADARSAT-1 Standard Beam 1 scene acquired using HH polarization over the same region on April 30, 2006 with approximately the same incidence angles.

To test whether different incidence angles affected our results, we compared images with shallow incidence angles from RADARSAT-1 Standard Beam 6 and 7 with ERS-2 scenes acquired the same days. While this test was not exhaustive, we did not see any noticeable difference in the percentage of lake area that was BI for the control, the polarization test or the incidence angle test up to 44° (Table 4). There was a slight difference in results using the steep incidence angle of ERS-2 and the shallow incidence angle of RADARSAT-1 Standard Beam 7 (47° at scene center): we noted this and therefore limited the incidence angles that we used in this study to ≤ 44° in the far range of some images over our sites. We concluded that our interactive threshold selection method provided results that could be compared between years imaged with different SAR parameters.

2.7. Accuracy assessment of SAR classification

To check the accuracy of our lake ice classification, we compared

Table 4
Results from comparison of SAR analysis results using data with different imaging parameters that were acquired co-temporally. Different co-polarizations did not affect our results since VV data and HH data acquired on the same date yielded nearly identical results. Differences in incidence angle yielded slightly different results in classification, and this study therefore limited incidence angle to avoid extreme steep or extreme shallow degrees, only using data acquired with incidence angles within the 21° to 44° range. Transitional and intermittent lakes are a multi-year classification and are built from the classification of FI and BI lakes for each year. Over 700 lakes in the Teshekpuk region were used for each test. Percentage of number of FI and BI lakes listed are result of automated classification only, prior to manual quality check.

SAR platform	Date	Central incidence angle (°)	Polarization	Percentage of lake area classified as FI/BI	Difference in percentage of ice regime area	Percentage of number of FI/BI lakes	Difference in percentage of number of types (FI/BI) lakes	Type of test
ERS-1	23-Mar-1996	23	VV	49.49/50.51	0.02	12.48/87.52	0	Control
ERS-2	24-Mar-1996	23	VV	49.51/50.49		12.48/87.52		
ERS-2	30-Apr-2006	23	VV	48.54/51.46	−0.13	11.93/88.07	0.14	Polarization
R1 Standard 1	30-Apr-2006	22	HH	48.40/51.60		11.79/88.21		
ERS-2	4-Apr-2008	23	VV	49.49/50.51	1.01	12.65/87.35	0.88	Incidence angle
R1 Standard 6	4-Apr-2008	44	HH	50.50/49.50		11.76/88.24		
ERS-2	20-Apr-2007	23	VV	51.63/48.37	−3.35	11.68/88.32	−0.90	Incidence angle
R1 Standard 7	20-Apr-2007	47	HH	48.28/51.72		12.57/87.43		

Table 5
Accuracy assessment shows C-band SAR-based classification of lake ice regimes as compared to results from measurements after drilling at a point location. April field measurements from 2008, 2009, and 2012–2016 are compared to classification results from ERS-2, Envisat ASAR, RADARSAT-2, and Sentinel 1a SAR. Overall accuracy is 93%, with 11 errors (combined Type 1 and Type2) out of 150 cases.

All regions	Bedfast ice, ground truth	Floating ice, ground truth	Total cases	Errors of commission (False positive, type I)
Bedfast ice, SAR	54	7	62	11%
Floating ice, SAR	4	85	88	4%
Total cases	58	92	150	
Errors of omission (Ignored cases, type II)	7%	9%		Overall accuracy: 93%

150 in situ measurements in the Teshekpuk, Fish Creek, Inigok, Umiat, and NSP regions from late March and April 2008, 2009, and 2012–2016 (Table 5, Fig. 4) to our SAR-based lake ice classification. Field measurements included ice thickness, water depth, probing sediments for the presence of taliks (thaw bulbs) and water salinity measurements. These data provided enough information to not only determine BI and FI conditions at a point location but to further delineate BI overlying unfrozen sediments and FI lakes with briney water (occurring near ocean) or just a few centimeters of high-salinity liquid water from salts forced into solution from the freezing process.

Using an ERS-2 April 1, 2008 image (Fig. 4) and SAR images acquired for 2012–2016 (Table 3), we calculated the intensity values of pixels nearest the GPS point of each drilling site using bilinear interpolation in ArcMap (v10.3). We compared this SAR intensity value to the threshold determined from each image and classified values lower than each scene's threshold as BI and values higher than the threshold as FI. We then compared this classification to the ground truth measurement at that point.

3. Results and discussion

3.1. SAR comparability, accuracy, and classification thresholds for long-term analysis

Our study yielded excellent accuracy when compared to point locations of field measurements in 2008, 2009, and 2012–2016. SAR correctly classified 139 of the 150 cases of lake ice (Table 5), resulting in an overall classification accuracy of 93%. Individual geographic regions' classifications ranged from 100% accuracy in Fish Creek (21 cases) to 87% overall accuracy in Inigok region (30 cases).

Of the 11 errors, two FI locations were misclassified as BI where detailed field measurements revealed high salinity, and four errors occurred where lakes deeper than four meters were misclassified as BI, although generally the accuracy rate for deeper lakes was good with 12 out of 16 correctly classified as FI. Another of the 11 classification errors was due to geolocation errors in a hilly region where micro-topography could be a challenge for SAR terrain correction. Three of the 11 misclassifications occurred on the northern Seward Peninsula where the ice was drilled through floating vegetation mats, which are formed where thermokarst subsidence along shorelines removes most of the soil underlying tundra vegetation which then floats on the lakes surface in large intact mats (Parsekian et al., 2011), indicating C-band SAR sensitivity to vegetation frozen in ice. The eleventh classification error was due to high σ^0 from a lake that was frozen to the bottom, yet had unfrozen lake bed sediments according to field measurements six days after SAR acquisition date. High SAR σ^0 from BI lakes with taliks has only recently been documented in published literature to our knowledge (Gunn et al., 2018), although unfrozen ground beneath BI lakes has been posited as a reason for higher σ^0 in BI lakes (Grunblatt and Atwood, 2014), only Gunn et al. (2018) has field data reporting

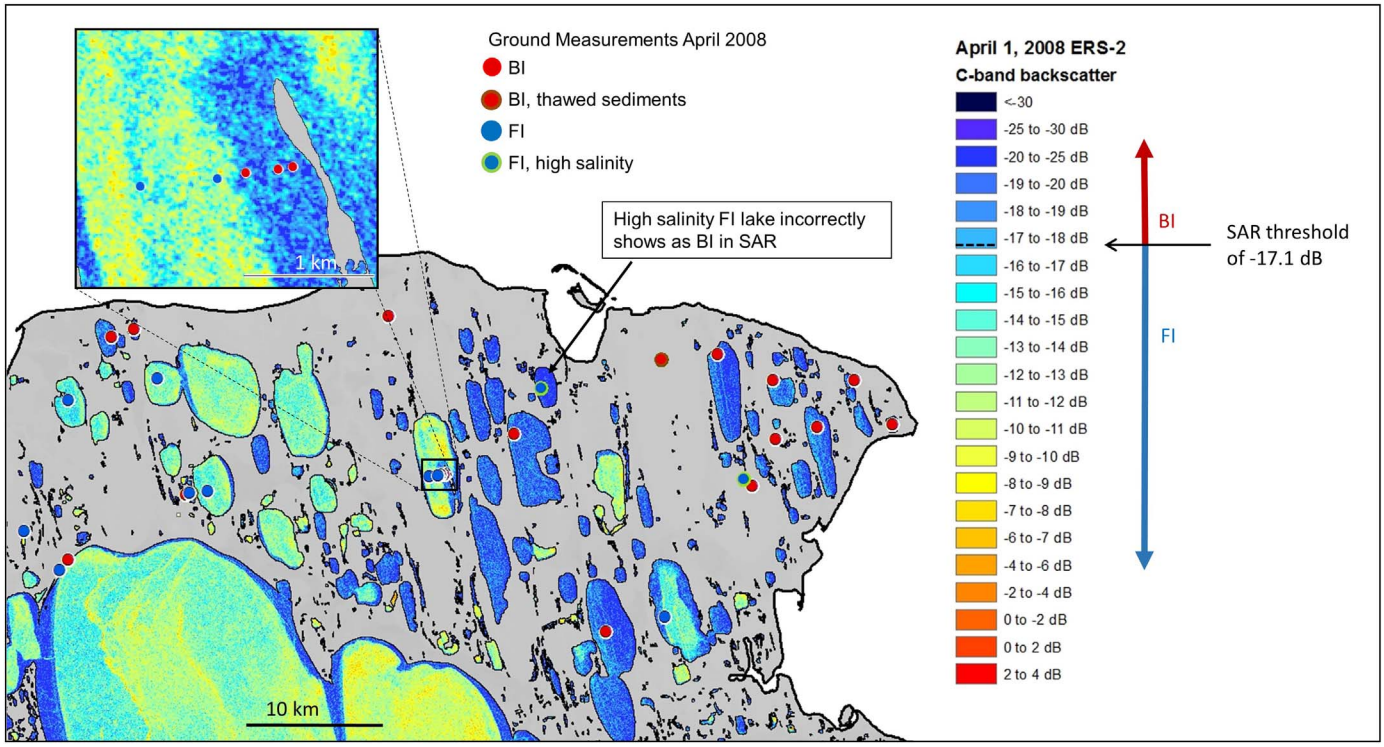

Fig. 4. SAR σ^0 from lake ice shown as colorized log-transformed (dB) values on Teshekpuk area landscape (land is grey). Ground measurements from April 1–8, 2008 are shown as red or blue dots. Our analysis agrees with ground measurements in 29 out of 32 locations for this year: two errors were due to FI with high salinity and one misclassified BI lake had an unfrozen talik. See also Table 5. We utilized 150 ground measurements over 6 years to test the accuracy of SAR-derived lake ice regimes. Dataset: ERS-2, © ESA 2008; retrieved from ASF DAAC August 2015.

unfrozen sediments under BI at a point with higher-than-expected σ^0 to support this consideration. Our new single case of false FI classification in a BI lake with unfrozen sediments is not enough data to determine if talik presence always causes higher σ^0 in BI lakes. We recommend future study, possibly paired with geophysical ground measurements, to determine if SAR σ^0 is consistently high for bedfast lakes with unfrozen sediments.

We were able to manually correct for many SAR classification errors for lakes deeper than 4-m using previously published depth data and lake depth measurements from 2008 to 2016 (Table 1), and using visual interpretation of optical imagery which often shows shallow shoulders and deep centers of lakes. We performed an additional manual check for misclassification of deep FI lakes by looking for a visually brighter ring around deep lake centers, where lake depth is < 4-m deep and thus exhibits bright FI. In cases of misclassification caused by geolocation errors, we were able to manually correct many by comparing ascending and descending passes and referencing high resolution optical satellite imagery to determine areas of shoreline with high bluffs that caused high layover backscatter within the lake perimeter in cases of imperfect geolocation. While it is not guaranteed that every error was elucidated, we were able to identify regions where deep lakes and imperfect image geolocation with SAR classification were most probable and intensified manual quality checks in these regions.

In the case of salinity > 2% (Mellor, 1982), we currently cannot visually detect and correct for BI misclassifications. High salinity in lake water can be caused by storm surges along coastlines. Also, the last few centimeters of liquid water under ice can be highly saline due to salts excluded from freshwater ice formation. Because of SAR's inability to distinguish between true BI lakes and high salinity FI lakes, the number of BI lakes and the BI area may be inflated if derived from SAR. We've noticed that often high salinity FI lakes have extremely low σ^0, possibly significantly lower than BI σ^0, but additional analysis would be needed to discriminate between low-backscatter BI lakes and low-backscatter high-saline FI lakes. We recommend further SAR analysis to determine differences in backscatter from BI lakes and high-saline FI lakes in order to correct landscape-scale SAR derived ice regime classifications.

Our novel method of using adaptive thresholds for each SAR scene from the frequency distributions of lake ice pixels allowed us to map lake ice regimes over 25 years: we could determine a perennial regime of FI or BI, or otherwise the change in each lake regime as either transitional or intermittent. This no-bias threshold method is more appropriate than fixed thresholds used in other studies (French et al., 2004; Grunblatt and Atwood, 2014) because it accounts for differences in SAR signal strength (Fig. 2) and differences in SAR incidence angle and polarization (Table 4). Additionally, a unique threshold for each scene accounts for differences in snow wetness and changes in bubbles and lake ice roughness at the ice/water interface (Atwood et al., 2015) which is the dielectric contrast that drives SAR high σ^0 from FI. A fixed, general threshold would not account for these differences between SAR scenes (Fig. 2).

3.2. Patterns and trends in lake ice regimes across Arctic Alaska

Analysis of late winter ice conditions of 11,571 lakes across seven regions of arctic Alaska totaling 15,250 km^2 over a 25-year period provided a rich dataset to dissect and discuss in the context of lake landscapes and permafrost vulnerability (Table 2). Over this 25-year period in our seven study regions, FI extent averaged 53% of the total lake area (2305 km^2) and 7% of the total landscape area (Table 6). For comparison, a single year 2009-census of lake ice on Alaska's North Slope found 51% of lake ice was FI (Grunblatt and Atwood, 2014). Comparing the Grunblatt and Atwood (2014) dataset to our study regions in the Arctic Coastal Plain (omitting Seward Peninsula) for 2009 shows agreement: 49% of lake area had FI in our study. The landscape-wide source of variation in any ice regime inventory is primarily the result of the depth distribution of water in lakes and the MIT which varies by almost 50 cm between northerly and southerly study areas (Table 1). However, many SAR lake-ice census studies assume a

Table 6
Proportion of lake area (LA) and total area (TA) with floating ice (FI) averaged over the study period (1992 to 2016), years with minimum and maximum extents of FI, and range of variation in FI area over this period. When < 1% difference in FI area divided extreme years, all years are listed. Full dataset can be found at https://doi.org/10.18739/A2FC5W.

Region	Average floating ice area		Extreme years of record		Range in floating ice area	
	% of LA	% of TA	Min.	Max.	% of LA	% of TA
Barrow	48.2	10.9	1992	1999, 2011, 2014	26.4	6.0
Teshekpuk	47.8	7.6	2000 & 1992	2014	13.9	2.2
Fish Creek	47.6	6.6	1992	2011	22.4	3.3
Kuparuk	19.8	2.4	2013	2003	30.8	3.7
Inigok	54.1	13.6	2013	2006 & 2011	17.3	4.4
Umiat	85.3	1.0	2013	1996	29.2	0.4
Seward Peninsula	68.5	4.5	1997	2008	27.4	1.9
All regions	53.0	6.6	–	–	23.9	3.1

consistent regional ice thickness based on models or limited field data. Our extensive field measurements show large interannual variation in MIT that is primarily responsible for changing lake ice regimes. Factors such as regional water balance and local lake drainage are typically considered secondary factors (Jones et al., 2009; Arp et al., 2012; Surdu et al., 2014). In this study the minimum FI extent occurred in either 1992 or 2013 for six of the seven regions, while maximum FI extent occurred in 2011 in the regions of Barrow, Fish Creek, and Inigok, but a common year of this maximum was not observed in other regions (Table 6 and Fig. 5). This pattern of the same minimum FI year across regions and the lack of a similar pattern for maximum FI year indicates that factors which cause less FI (e.g. colder air temperatures, thinner snow-cover, and drought) span a larger geographic area comprised of several regions, while factors causing more FI (e.g. either thinner ice caused by thick insulating snow-cover or deeper water caused by heavy late summer rainfall) differ more between regions in a given year. The areal extent of all lakes in our study regions over this 25-year period showed 24% of lake area had FI in some years but was bedfast in others (Table 6). Thus, there may exist a relatively large zone of surface water where the ice regime and sub-lake permafrost may be changing or variable across the Arctic landscape. This dynamic zone for each region ranged from 14 to 31% of total lake area that has not been frozen in some years due to the presence of liquid water and where new taliks may be developing (Table 6). Expressed in terms of area of landscape affected/susceptible to thaw as a result of change from BI to FI, the values range from 0.4% of the land area in the Umiat region to 6% of the land area in the Barrow area with a mean for all regions of 3% of the land area among all study regions (Table 6). Such areas that vary or shift between FI and BI should be most sensitive to rapid shifts in thermal conditions and other corresponding biogeochemical and ecological processes (Arp et al., 2016). (See Fig. 6.)

Characterizing a lake by ice regime, whether it freezes entirely to its bed throughout (i.e., bedfast ice regime) or retains some liquid water below FI even if in small amounts (i.e., floating ice regime), provides a basis for predicting potential overwinter fish habitat, refuge for other freeze-intolerant biota, availability of liquid water for industrial or municipal uses, and where water bodies are most prone to sub-lake permafrost thaw (Brewer, 1958; Jones et al., 2009). The majority of lakes among our study regions were classified as Stable BI regimes across our 25-year study period, though Stable FI lakes accounted for the majority of lake area (Table 7).

Traditionally, only two classes of lake ice regime (BI or FI) have been used based on individual years using extensive ice coring or surface geophysical measurements near the period of MIT, or more commonly using late winter SAR acquisition and classification (Mellor, 1987; Jeffries et al., 1996). An additional class of ice regime, intermittent or transitional, was added by Arp et al. (2012) using a 9-year time series of ASAR imagery acquired in late winter to also identify lakes that had BI in some year and FI in others. Our study greatly expands the ability to rigorously identify intermittent and transitional ice classes by looking at a much longer time period that was enabled by our novel image classification approach.

Intermittent lakes, which vary between BI and FI conditions without detectable trends over the 25-year period, accounted for a large portion of ice regimes, 12% of lakes and 14% of lake area across all study regions (Table 7). Lakes transitioning directionally from bedfast ice to floating ice regimes (TRANS-FI) accounted for 2% of lakes and 2% of lake area. This class of lake ice regime are those considered to be responding to trends in thinning ice coupled with lake depth distributions within the range of inter-annual variation in MIT (Arp et al., 2012; Zhang and Jeffries, 2000). These lakes coupled with other intermittent

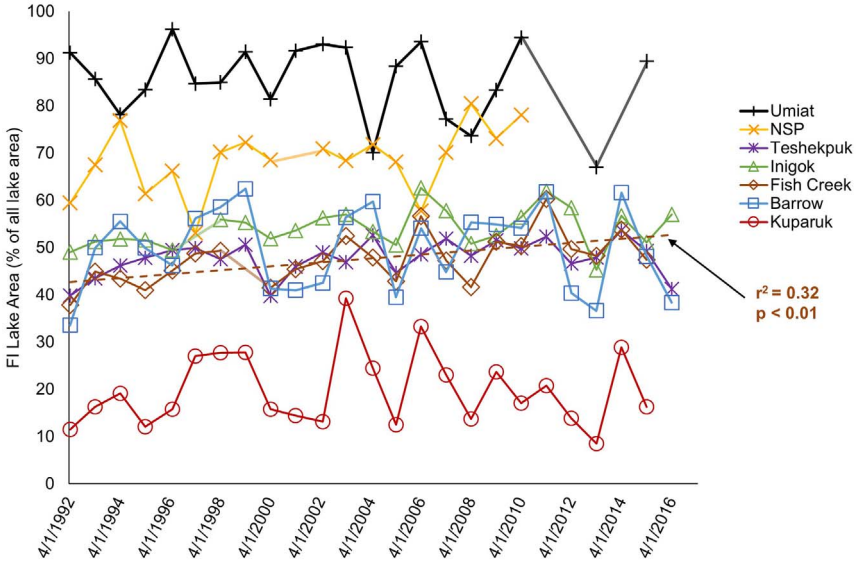

Fig. 5. Results from SAR-based lake ice regime classification for seven geographic regions in Alaska, USA. The percent of lake area across the landscape that has floating ice (FI) for each year varies between regions and years. Fish Creek (shown in brown) was the only region that showed a significant trend in area of FI over time.

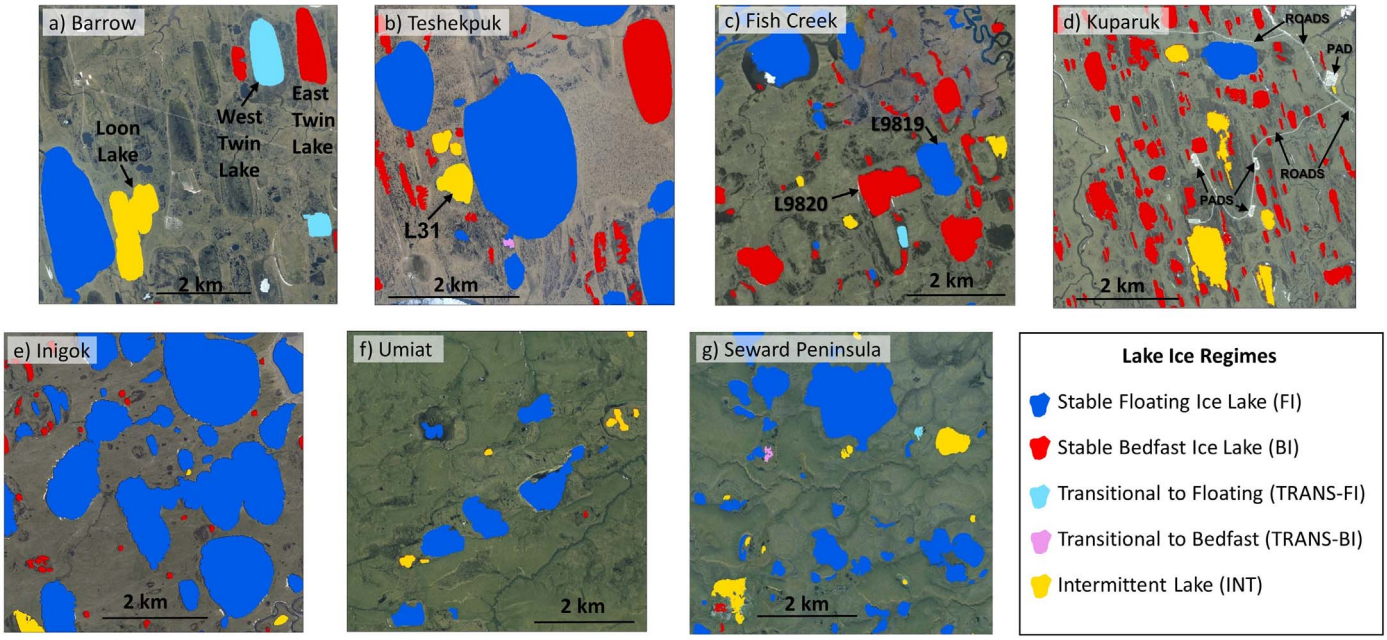

Fig. 6. Determination of prevailing ice regime. Blue shows a floating ice (FI) regime in the lake for 90% or more of the years studied, cyan shows ice the regime transitioning from bedfast to floating, red shows a bedfast ice (BI) regime for 90% or more of the years studied, pink shows the ice regime transitioning from floating to bedfast, and yellow shows an intermittent lake ice regime where a lake is sometimes FI and sometimes BI, but with no trend over time. Panel a) shows West Twin lake is a TRANS-FI lake, b) shows L31 as an INT lake, c) shows L9819 is FI and L9820 is BI, d) shows roads and pads of petroleum industry among INT, Stable BI, and Stable FI lakes, e) mostly Stable FI lakes due to lakes with deep centers, f) shows mostly Stable FI lakes in foothills, and g) mostly Stable FI lakes with small pink TRANS-BI lake and small cyan TRANS-FI lake. Background image is SPOT statewide ortho map from http://gis.dnr.alaska.gov/.

lakes drove the decline in the number of bedfast ice lakes, though only lakes in Fish Creek were found to have a significant decline (at the rate of 1.5 lakes/10 years, $r^2 = 0.23$, $p < 0.05$) over the period analyzed. Lake-rich regions most surrounded by coastline, Barrow and Seward Peninsula, also showed a wide range of intermittent lake ice regimes that may be responding to dynamic sea ice conditions, which have been shown to impact early winter ice growth (Alexeev et al., 2016). A slightly smaller number of lakes, < 1%, were responding in the opposing direction, shifting from floating ice to bedfast ice regimes (TRANS-BI), though these accounted for a slightly larger aerial extent, > 2% (Table 7). Lakes in this TRANS-BI class are most likely responding to lower lakes levels caused locally by partial lake drainage from geomorphic changes or possibly due to watershed changes that reduce water balance (Jones et al., 2009; Arp et al., 2011).

3.3. Ice regime dynamics by study area

3.3.1. Barrow peninsula

Lakes on the Barrow Peninsula have been well studied because of their abundance, thermokarst origin, and striking orientation (Black and Barksdale, 1949, Carson and Hussey, 1962, others). Brewer (1958) first observed differences in ice regimes of lakes here noting two distinct classes of lakes either having depths of about 1 m or less with BI, or depth of 2 to 3 m with FI regimes. We selected the boundaries of the Barrow Peninsula study area to match those of Surdu et al. (2014). Our analysis of 2228 lakes covering 23% of the landscape in our Barrow Peninsula study region showed roughly half of the lake area had FI over this study period (Table 6 and Fig. 5). This FI extent however varied greatly from year to year ranging from 34% FI in 1992 to approximately 60% FI in years 1999, 2011, and 2014 (Fig. 5) resulting is 6% of the total landscape area covered in perennial liquid water in some years and not others (Table 6)—the highest percentage of variation in FI area for any of our study landscapes.

Our observations follow similar ERS-1 SAR inventories by Jeffries et al. (1996) showing 23% FI lake area and Surdu et al. (2014) showing 38% FI lake area in 1992, with the latter domain more closely matching that of our study. Using the same SAR scenes as did Surdu et al. (2014), our methods allowed us to classify smaller lakes down to the size of 1 ha, increasing the number of lakes that we classified. Using a subset of our lakes that matched the 402 larger lakes in the Surdu et al. (2014)

Table 7
Lake classification of ice regime by number (%No.) and areas of lakes (%Area) using multi-temporal synthetic aperture radar imagery. Lakes without stable ice regimes over this period were either classified as Transitional (BI to FI) or Transitional (FI to BI) if a significant trend from one regime to the other was detected, or Intermittent if no significant trend was detected. Standard deviation of the mean for all regions is shown in parenthesis.

Region	Stable floating ice lakes		Stable bedfast ice lakes		Transitional (BI to Fl)		Transitional (FI to BI)		Intermittent lakes	
	%No.	%Area	%No.	%Area	% No.	%Area	% No.	%Area	%No.	%Area
Barrow	12.2	38.9	70.4	14.0	6.4	4.2	0.6	7.8	10.4	18.4
Teshekpuk	9.9	51.0	84.4	37.5	1.1	0.5	0.7	0.2	3.9	10.7
Fish Creek	24.7	68.4	67.3	18.7	2.6	4.4	0.3	1.4	5.1	7.1
Kuparuk	3.6	12.1	84.2	48.2	0.3	0.3	0.2	2.3	11.7	36.8
Inigok	48.9	93.6	43.3	4.1	0.7	0.1	0.3	0.02	6.7	2.1
Umiat	69.1	89.3	1.6	0.2	1.6	1.6	0.8	0.1	26.8	8.8
Seward Peninsula	67.2	79.5	10.5	5.7	0.8	0.2	1.4	4.1	20.1	10.5
All regions	33.7 (27.8)	61.8 (29.6)	51.7 (34.1)	18.3 (18.1)	1.9 (2.1)	1.6 (1.9)	0.6 (0.4)	2.3 (2.8)	12.1 (8.5)	13.5 (11.4)

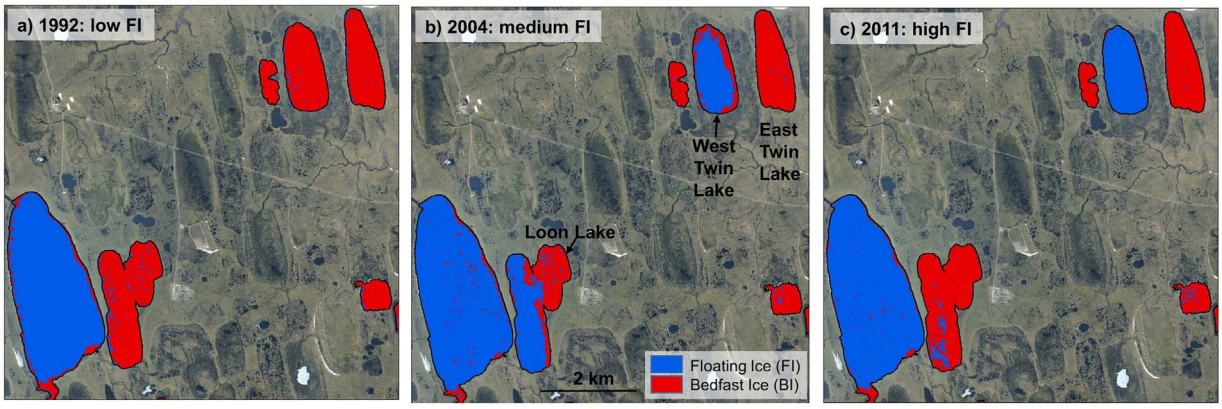

Fig. 7. SAR-based lake ice regime classification of lakes in the Barrow Peninsula study region showing a) low floating ice (FI) in 1992, b) medium FI in 2004, and c) high FI in 2011. Loon Lake shows individual variation, showing less FI in a high FI year than in a medium/average year. This could be caused by either lack of insulating snow resulting in thicker ice or a change in hydrology. Background image is SPOT statewide ortho map from http://gis.dnr.alaska.gov/.

study, maximum FI extents in our study very closely match Surdu et al. (2014) observations of 66% in 1999, and compared to 62% in our analysis, and to a lesser degree in 2011 of 74% compared to 62% in our analysis. Slight variation in lake perimeter shape and perhaps more importantly changes in the ERS-2 signal we detected and accounted for in our analysis may explain these slight differences.

Though no significant trend was detected in either ice condition by lake area extent, nor in lakes by ice regime over this study period (Fig. 5), sharp declines over a slightly shorter period highlighted by Surdu et al. (2014) will likely continue most profoundly on the Barrow Peninsula in response to rapid changes in early winter climate and sea ice (Wendler et al., 2014) and the connection to lake ice regimes (Alexeev et al., 2016). Taken together, intermittent and TRANS-FI lakes accounted for 17% of lake by number and 23% of lake by area over this 25-year period (Table 7).

Lakes transitioning from BI to FI (TRANS-FI) were generally smaller than their counterpart TRANS-BI, and accounted for 6% of lakes and 4% of lake area. An excellent example of such lakes is shown in Fig. 7a, where West Twin Lake had a BI regime in 1992, but has since consistently transitioned to a FI regime in medium and thin MIT years of 2004 and 2011, respectively. The adjacent and shallower East Twin Lake had a consistent BI regime over these same years (Fig. 7a). One percent of the lakes transitioned to BI regimes (TRANS-BI), however, these were relatively large lakes and thus impacted 8% of the lake area (Table 7). Lakes classified as TRANS-BI are most likely transitioning due to partial lake drainage in relation to thermokarst lake expansion into lower elevation shorelines, which could be more common in larger lakes because of higher shoreline erosion rates (Arp et al., 2011).

Predictions of the impact of these changes in lake ice thickness relative to lake depth for the Barrow Peninsula include increased thaw in sub-lake permafrost (Arp et al., 2016), which is at least partly driven by warmer and snowier early winters caused by lower sea ice extents of the Beaufort and Chukchi seas buffering the Barrow Peninsula (Alexeev et al., 2016).

3.3.2. *Teshekpuk*

The study area north of the very large (840 km^2) Teshekpuk Lake (Fig. 1) shares many similarities to the Barrow Peninsula in that it is part of the outer coastal plain, though mostly a younger terrain unit (Hinkel et al., 2005). Lakes in this region are predominantly thermokarst in origin and many of which are oriented similar to the Barrow Peninsula (Jones et al., 2009). The 697 lakes observed in the Teshekpuk region cover 16% of the landscape (Table 2). Approximately half of the lake area was covered with FI on average during our study period (Table 6). Although the averaged FI distribution is similar to that found on the Barrow Peninsula, the variation in FI extent was found to be lower, 14% of lake area and about 2% of the total landscape area. This is in comparison to nearly twice this variation FI extent on the Barrow Peninsula (Table 6). Classification of lakes by ice regime also followed the same pattern as found on the Barrow Peninsula with larger and fewer Stable FI lakes and smaller and more abundant Stable BI lakes (Table 7). Combined, intermittent and TRANS-FI lakes accounted for a much smaller number, 5%, and area, 11%, of all lakes compared to the Barrow Peninsula (Table 7), which follow similar observations for shorter 9-year (2003 – 2011) classification lake ice regimes for this area (Arp et al., 2012). Though the majority of dynamic classes in the

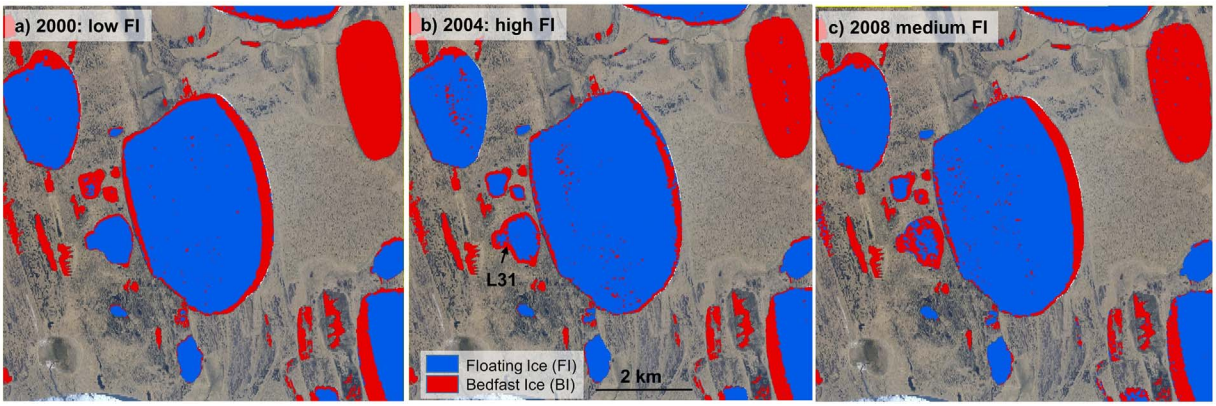

Fig. 8. SAR-based lake ice regime classification of lakes in the Teshekpuk Lake study region showing a) low floating ice (FI) in 2000, b) high FI in 2004, and c) close to average FI in 2008. The small lake L31 joined and partially drained into the large lake to the east, thereby showing less FI in panels b) and c) than in the year with low FI in panel a). Background image is SPOT statewide ortho map from http://gis.dnr.alaska.gov/.

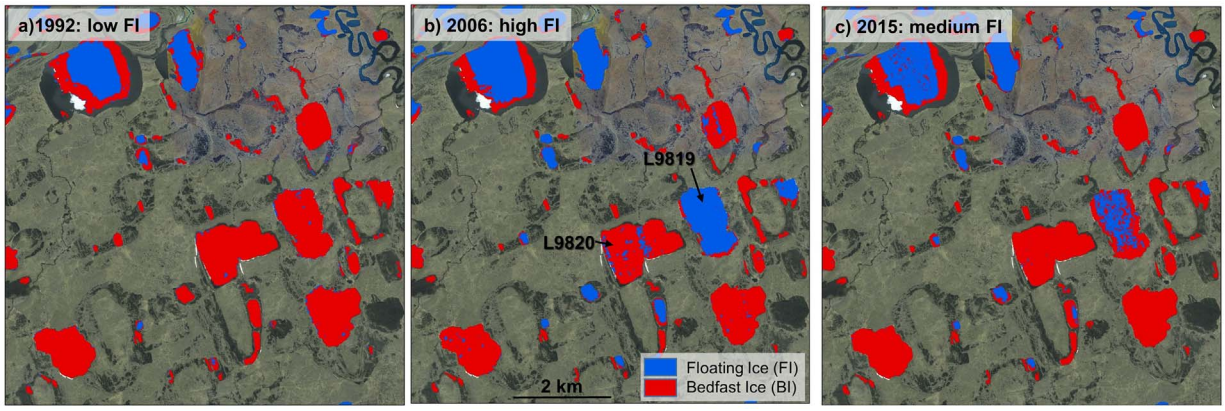

Fig. 9. SAR-based lake ice regime classification of lakes in the Fish Creek study region showing a) low floating ice (FI) in 1992, b) high FI in 2006, and c) medium FI in 2015. L9819 and L9820, labelled in panel b) are nearly the same depth, averaging 1.8 and 1.1 m respectively in field measurements from 2012 to 2016. Lakes with this one- to two-meter range of lake depth are vulnerable to changing ice regimes. Background image is SPOT statewide ortho map from http://gis.dnr.alaska.gov/.

Teshekpuk region were either INT or TRANS-FI, notable TRANS-BI examples exist such as Lake 31 (Fig. 8), which became bedfast due to recent lake tapping and partial drainage as described in Jones et al. (2009).

Observations of two distinct depth distributions by Brewer (1958) perhaps are more applicable for the Teshekpuk region than on the Barrow Peninsula based on our analysis, making this an ideal landscape to investigate detection and functioning of BI and FI lakes. Ground truth measurement during the 1976 campaign in fact recorded one of the thickest MIT measurements, 2.3 m (Weeks et al., 1978), documented for the Alaskan Arctic, and we can see MIT has decreased in recent years in the Teshekpuk region with measurements of 1.4–1.8 m (Table 1). Yet no significant decline FI extent (Fig. 5), nor number of FI lakes was observed over our 25-year study period. More recent studies in the Teshekpuk region have used this contrasting and stable distribution of BI and FI regimes to identify relationships with lake expansion rates (Arp et al., 2011), lake bed temperatures (Arp et al., 2016), and ice-out timing and corresponding water balance variation between ice regimes (Arp et al., 2015). Large lakes with distinct FI and BI regimes make the Teshekpuk area a site with ideal conditions to examine radar detection of fresh liquid water compared to BI or saline water.

3.3.3. Fish Creek

Lakes set within the landscape of the Fish Creek study area are of particular interest because this region is managed as part of the National Petroleum Reserve – Alaska (NPR-A) where petroleum exploration and development are active. Water for building winter ice roads and other industrial activities is supplied primarily from FI lakes, making their distribution and dynamics of economic and environmental interest (White et al., 2008; Jones et al., 2009; Jones et al., 2017). In contrast to the Teshekpuk and Barrow Peninsula regions, Fish Creek is located on the Inner ACPnA (Hinkel et al., 2005) with distinctly lower ice-content permafrost and much smaller lakes of both fluvial and thermokarst origin (Jorgenson and Shur, 2007; Jones et al., 2017). We observed 1331 lakes in this region covering 15% of the total area (Table 2) with approximately half the lake area existing as FI on average and intermediate range of variation in FI extent, 22%, (Table 6) compared to the previously discussed Outer ACPnA regions. Minimum FI extents were observed in 1992 and maximum FI extents were observed in 2011, similar to the Barrow Peninsula (Table 6). Most lakes with BI regimes were small, accounting for 19% lake area, but 67% of all lakes numerically (Fig. 5 and Table 7). Thus most lakes in this region can only supply ice chips for industrial uses and only provide summer habitat for fish (Jones et al., 2017). Finer-scale late winter radar analysis of a portion of Fish Creek in late winter 2013 using 1.25-m TerraSAR-X identified that 42% of water body area could provide potential overwinter habitat including fluvial systems (Jones et al., 2013) with lake area classification comparing very well to the same year in our analysis.

Though changes in FI extent from 1992 to 2016 visually show increasing trends for many regions studied, only lakes in the Fish Creek region had a significant increase 4.2%/decade ($r^2 = 0.32$, $p < 0.01$) in areal extent (Fig. 5) and 1.5%/decade by number of lakes with FI ice regime ($r^2 = 0.23$, $p < 0.05$). A significant increase in FI was also observed in a shorter-term data set (9-years) in this region using ASAR imagery (Arp et al., 2012). We suggest that lower interannual variation explains this significant trend in Fish Creek and is most related to a tighter range of lake depth distributions around the average MIT of 1.5 m (Table 1). In other regions, a larger proportion of lake area is either much shallower or much deeper than average MIT likely cause either greater variation or minimal response to thinning lake ice. Three percent of the lakes by area are TRANS-FI in Fish Creek, higher than the average for all regions (2%) and second only to the Barrow Peninsula region, with very few TRANS-BI class lakes in Fish Creek, < 1% (Table 7). Analysis of shifting lake ice regimes in the Fish Creek region was enhanced by comparison of recent multi-year classification to a 1980 synoptic airborne radar classification showing numerous lakes shifting ice regimes (Arp et al., 2012), while few were discovered in comparing the same data sets in the Teshekpuk region.

A prime example of a FI lake, L9819, and its impact on both petroleum development and fish habitat is shown in Fig. 9. This lake has a maximum depth of about 1.8 m and froze completely in 1992, but has demonstrated consistent FI conditions in all years since, whereas the adjacent lake, L9820, is about 1.2 m maximum depth and has had consistent BI conditions in all but a few years (Jones et al., 2013). Both lakes provide summer fish habitat (Heim et al., 2015) and L9819 has recorded dissolved oxygen levels suitable for overwintering in recent years (Leppi et al., 2015). A new oil drilling platform being installed just north of these lakes makes these particular lakes valuable resources for winter water supply. This lake, L9819 may not have been a reliable water source several decades earlier, nor could it have provided reliable overwintering fish habitat (Fig. 9).

3.3.4. Kuparuk

Of the 2548 lakes observed in the Kuparuk region covering 12% of this part of the Inner ACPnA (Table 2), BI extent dominates with 84% of lakes freezing solid on average (Table 7). This result closely matches synoptic late winter published SAR analysis in this region for March 2006 and likely are representative of most Alaskan coastal plain areas east of the Colville River (White et al., 2008). This area has been heavily developed for oil production beginning in the 1970's well before this 25-year observational period initiated (Streever, 2002). Drilling pads

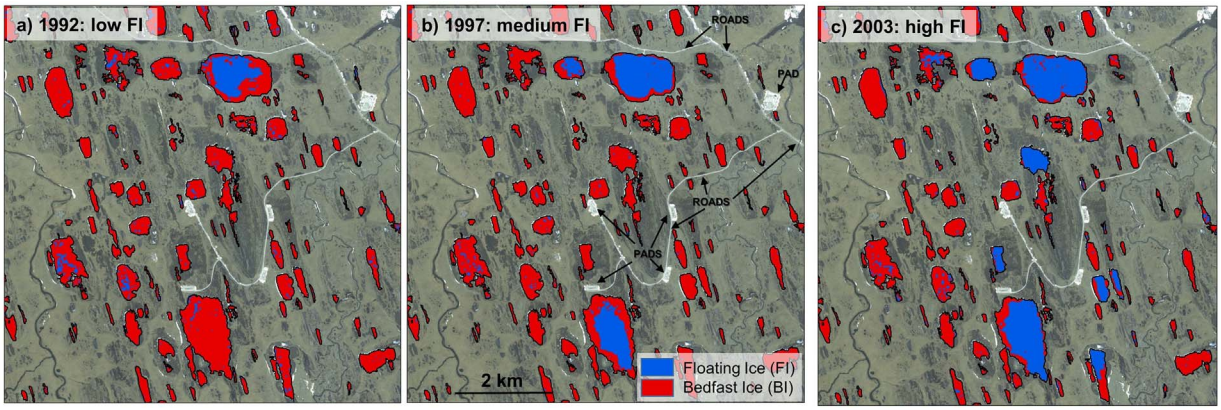

Fig. 10. SAR-based lake ice regime classification of lakes in the Kuparuk study region showing a) low floating ice (FI) in 1992, b) medium FI in 1997, and c) high FI in 2003. Roads and pads in the background image are associated with the oil development industry. Background image is SPOT statewide ortho map from http://gis.dnr.alaska.gov/.

and roads, both permanent and temporary winter ice roads built mainly from lake water, are interspersed with many small shallow lakes (Fig. 10). Despite a very small (12%) average area of FI (Table 7), this area shows the widest range of variation of all study regions—the recent thick ice year of 2013 had only 9% FI area and 2003 had 39% FI area (Fig. 5). This wide range is likely a function of many shallow lakes that minimally exceed the MIT (Table 1). Only a small number, < 4%, of lakes had Stable FI regimes over this period, but these lakes were proportionally larger than average, accounting for 12% of lake area (Table 7). Few lakes were observed to be transitional in this region, but many were intermittent, 12% of lakes covering 37% lake area.

The shallow depth distribution, inferred by the large percentage of Stable BI regime of Kuparuk lakes coupled with high ice regime intermittency suggests either high variation in MIT or possibly high variation in lake water levels. Thus variance in lake depth distributions exists, perhaps to a much greater extent than other regions. Previous analyses of the relative role of lake ice thickness compared to water balance suggests that variation in MIT driven by winter temperature and snow dominates (Zhang and Jeffries, 2000; Arp et al., 2012). However, watershed studies of the nearby Putuligiuyak River that drains a portion of the ACPnA near the Kuparuk suggest wide interannual variation in lake area extent as driven by snowpack and a thin balance between summer rainfall relative to evapotranspiration (Bowling et al., 2003). Lake storage deficit is viewed as a key driver of runoff explaining a widening range of runoff responses in ACPnA watersheds in recent years and perhaps relating to our observations of high interannual variation in FI extent.

Evaporation rates are known to be higher from BI lakes due to earlier ice-out compared to FI lakes (Arp et al., 2015), making lakes in the Kuparuk area more sensitive to summer warming. Another potential factor that deserves exploration is that much lake water in this area is extracted for ice road construction and other industrial activities, the latter of which occurs both in the summer and winter. Local lake level drawdown could explain some the higher level of intermittent behavior in this region, which is the highest by area of all regions in this study: 37% by area compared to a mean of 14% for all regions. Water extracted from lakes does not necessarily leave the region and may flow back into the same or other lakes once ice roads melt in the spring, but such activities may cause more variation in water balance than naturally occurs in other regions we studied.

3.3.5. *Inigok*

Although the Inigok region is also a part of the Inner ACPnA (as are the Fish Creek and Kuparuk regions), the Inigok region is distinct in that this terrain is draped with a vegetated sand sheet known as the Pliestocene Sand Sea (Carter, 1981) with abundant lakes set between dune crests. Most of these lakes have deep central basins with wide shallow sand shelves. Lakes with this morphology may have a thermokarst origin (Grosse et al., 2013) or originate simply as depression lakes in the undulating topography (Jorgenson and Shur, 2007). Such lakes account for the majority of the surface area in this region, while other mostly fluvial lakes may account for much of the lake density (Jones et al., 2017). Lakes in the Inigok study area (Fig. 11) pose a challenge for ice regime classification with SAR since many of the lakes have a depth > 4 m in central basins and present a low-backscatter SAR signal similar to BI (Mellor, 1982). White et al. (2008) noticed this

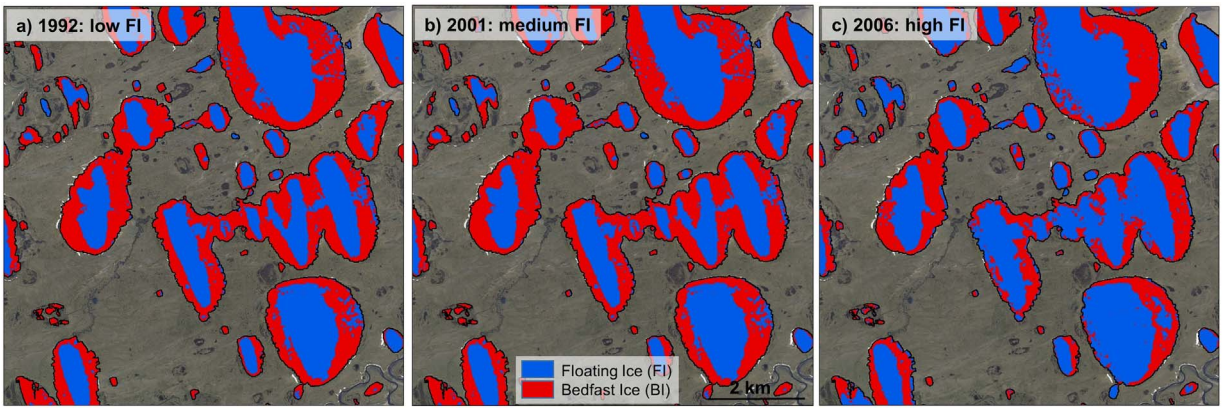

Fig. 11. SAR-based lake ice regime classification of lakes in the Inigok study region showing a) low floating ice (FI) in 1992, b) medium FI in 2001, and c) high FI in 2006. The deep centers and shallow shoulders of these lakes can be clearly seen as they demonstrate ice regime variability within the lakes between years. Background image is SPOT statewide ortho map from http://gis.dnr.alaska.gov/.

ambiguous signal and declared some lakes undeterminable in the Inigok region. We used published lake depths and our own field measurements in conjunction with extensive manual SAR interpretation in this region to correct this problem.

Lake area extent in the Inigok region is the highest, 26%, among our seven study areas (Table 2) and dominated by Stable FI lakes accounting for 49% of lakes by number and 94% by area (Table 7). Accordingly, classification of lakes for winter water supply suggests abundant resources if development in the NPR-A progresses farther west into the Inigok or similar sand sea regions of the North Slope (Jones et al., 2017). Floating ice extent averaged 54% over the 25-year study period ranging from 63% in 2006 to as low as 45% in 2013 (Table 6 and Fig. 5). Much of this variation is likely associated with the lake margins of sloping sand shelves that freeze solid in thick ice or low water-level years and remain unfrozen during opposing conditions (Fig. 11). Only 2% of lakes by area were classified as intermittent in this region (Table 7), although the large areal extent of the distinctive shallow shoulders of the deep lakes in the Inigok region probably account for the relatively high variation in FI area, 4% of total landscape area (Table 6).

3.3.6. Umiat

In contrast to the Inigok region, Umiat lakes in the Brooks Range northern foothills occur at comparatively very low areal extent, 1%, with only 123 lakes observed in our 1100 km^2 region (Fig. 1 and Table 2). Though much lower in abundance, many are relatively deep owing to high ice content of syngenetic permafrost in eolian loess, termed yedoma, with potentially high methane emission rates (Walter et al., 2006). Most lakes here are likely of thermokarst origin with others forming due to fluvial processes along river floodplains. Few previous studies have examined lake ice processes or lakes in general in this region.

We found that an average of 85% of the lake area in the Umiat region was FI over our study period (Table 6) and ranged from 96% in 1996 to 67% in 2013 (Fig. 5). Classification of lakes by ice regimes over this period showed that 69% of lakes always had FI and these accounted for 89% of lakes by area (Table 7). The largest lake in this low lake density region had one deep portion that comprised over 5% of the total lake area and remained perennially FI, while the majority of the lake oscillated between varying degrees of FI and BI (Fig. 12). Less than 2% of lakes could be classified as Stable BI and were very small, accounting for only 0.2% of lake area. Few lakes were distinguished as transitional, but a relatively high number, 27%, were INT over this period and these were small as well, comprising only 9% of lake area (Table 7). Maximum ice thickness averaged 1.5 m in this region (Table 1), yet can be much thinner in some years, such as 2015 when average observed MIT was about 1.0 m (Arp et al., 2016). Often deeper snowpack occurs in this region of the foothills causing much slower ice growth and likely drives most of the intermittency in lake ice regimes of this region.

3.3.7. Seward Peninsula

Lakes on the northern Seward Peninsula are thermokarst in origin with steep, high banks where the lake resides in undisturbed soils and low banks in areas of the lake that overlap with previously drained lake basins. Permafrost in this area is ice-rich (Table 2) and is also carbon-rich, due to sudden freezing in the Pleistocene (Farquharson et al., 2016), resulting in a high rate of lake-sourced methane (Engram et al., 2012). The majority of lakes on the northern Seward Peninsula region display Stable FI regime, 67% by number and 80% by area with only a small number of small lakes (11% by number and 6% by area) displaying Stable BI conditions (Table 7). The variation in FI lake area was 27% (Table 6), indicating that over one-fourth of lake area has fluctuated between BI and FI sometime over the study period from 1992 to 2013 and thus susceptible to talik (thaw bulb) creation. Less than 1% of the lakes are transitioning from BI to FI, but a larger area of lakes (4%) has transitioned from FI to BI (Table 7), due to several large (> 1 km^2) lakes partially draining in this region between 1950 and 2007 (Jones et al., 2011; Regmi et al., 2012).

Although the percentage of landscape covered by lakes at 7% is much lower in this region than the 18% on the Arctic Coastal Plainof northern Alaska (Table 2), northern Seward Peninsula is an active thermokarst lakescape, characterized by abundant drained lake basins (75% areal extent) (Jones et al., 2012) and lakes experiencing horizontal expansion especially into low-bluff shoreline lowlands (Jones et al., 2011). SAR-based lake ice classifications provide information about post-thermokarst soil deposition: we noted that an area of the southeast shore of Luna Lake with a high expansion rate (~50 m) from 1951 to 2006 (Jones et al., 2011) was BI in 1992–1996, then oscillated between BI and FI (1997–2002). Finally, the rim of new lake-area remained FI from 2003 to 2010, indicating that thermokarst action can turn lowland bluff soils into FI lake in at least seven years.

Unlike the lakes in Inigok, which have deep, oriented trough centers abruptly dropping off from shallow margins, or the Outer ACPnA regions of Barrow and Teshekpuk where lake beds generally taper from shallower margins to slightly deeper lake centers, the pattern of lake depth on the northern Seward Peninsula has little to do with the shape of the lake. There was no pattern of deep FI lake centers with BI near shorelines in this region. Nor was the variance of intra-lake ice regime related to the proximity of highland bluffs or lowland shores (Fig. 13) since there were many cases of FI near both types of shoreline.

4. Conclusions

We used C-band SAR data from ERS-1/2, RADARSAT-2, Envisat,

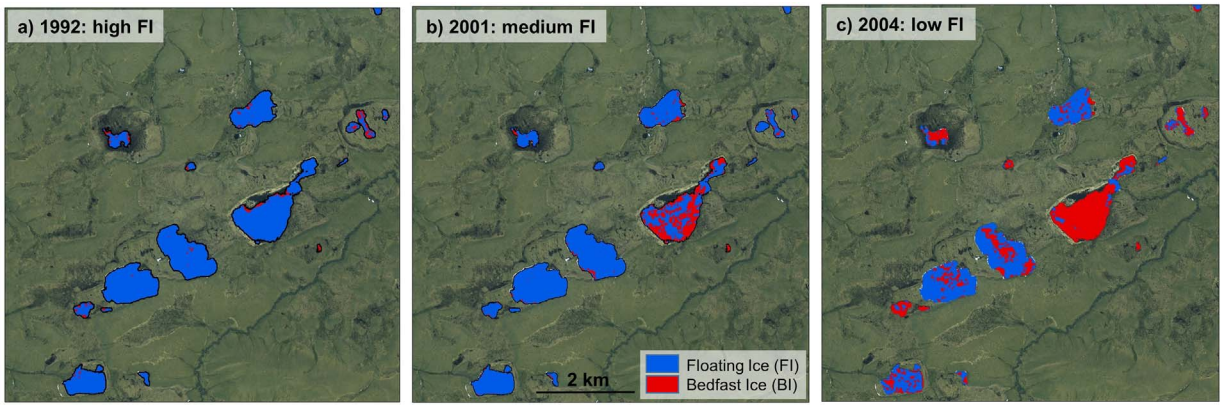

Fig. 12. SAR-based lake ice regime classification of lakes in the Umiat study region showing a) high floating ice (FI) in 1992, b) medium FI in 2001, and c) low FI in 2004. Large lake in right center of panels demonstrates wide variability in lake ice regime, yet retains enough FI in all years to be classified as a stable FI lake. Background image is SPOT statewide ortho map from http://gis.dnr.alaska.gov/.

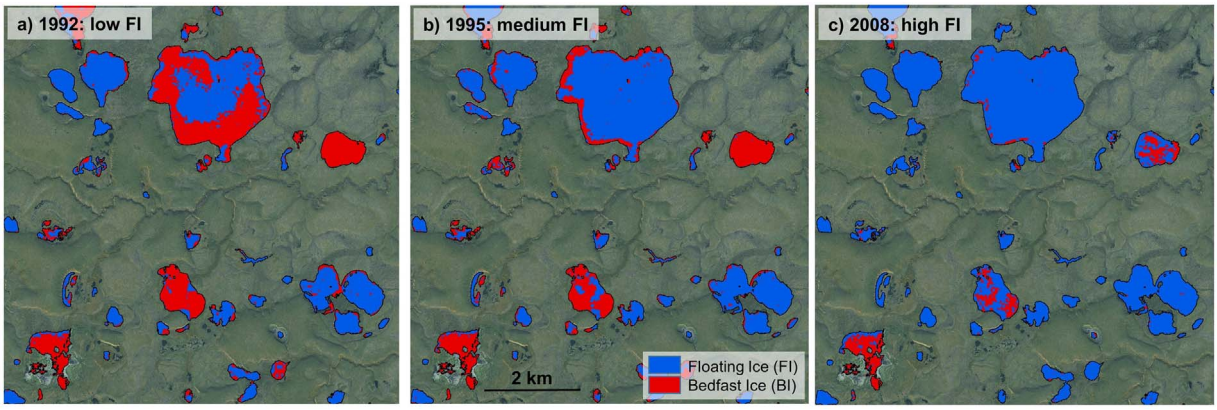

Fig. 13. SAR-based lake ice regime classification of lakes in the northern Seward Peninsula (NSP) study region showing a) low floating ice (FI) in 1992, b) medium FI in 1995, and c) high FI in 2008. Note patterns of FI are not in always in the center of lakes, nor do FI areas coincide with upland/lowland classification of adjacent shore. Background image is SPOT statewide ortho map from http://gis.dnr.alaska.gov/.

and Sentinel-1 to measure late winter FI extent on lakes and classify lake ice regimes in seven distinct regions of Arctic Alaska from 1992 to 2016. This multitemporal analysis effectively used overlapping SAR instruments with differing polarizations, incidences angles, and declining signal strength (ERS-2) with multiple years of field verification data and a novel no-bias threshold classification method to create a robust time series of lake ice regimes spanning 25 years. The record allowed us to assess long-term changes in lake ice conditions during a time when winter climate and lakes have undergone rapid changes in Arctic Alaska with the expectation of declining MIT and more FI regimes. We discovered, however, that high levels of interannual variability in FI extent and number of FI lakes obscured statistically significant trends toward more FI area and more FI lakes in six of the seven regions. The exception to this pattern of low signal to high noise was the Fish Creek region on the Inner ACPnA where FI area and number of FI lakes significantly increased over the last 25 years, matching results from Arp et al. (2012) for a much shorter time period. For the Barrow Peninsula region where much previous work has focused on lake ice dynamics (e.g., Jeffries et al., 1996; Zhang and Jeffries, 2000), we observed a similar increase in FI area from 1992 to 2011 as reported by Surdu et al. (2014), however the longer time span until 2016 did not yield a significant increase in either FI areal extent or number of FI lakes due to relatively thick ice in 2012, 2013, and 2016. Continued late winter SAR observations using robust techniques will be needed to determine if and when such high interannual variability in lake ice more consistently shifts to new regimes as has been predicted (Arp et al., 2012).

We highlight the utility of C-band SAR to monitor lake ice regimes and to quantitatively map the area of lakes that shift from bedfast to floating, whether oscillating or transitioning from one regime to another, and thereby show the amount of landscape undergoing permafrost thaw beneath lakes. We add to the literature another instance of high σ^0 from BI with thawed sediments corroborated by field measurements and underscore the possibility of future direct measurements of permafrost thaw via taliks using remote sensing, possibly with polarimetric C-band or L-band SAR data. We report for the first time that C-band SAR frequency interacts with macro-flora frozen in lake ice, indicating that frozen vegetation in ice could be a confounding factor to lake ice studies using this radar frequency.

In the absence of detecting consistent trends in Arctic lakes, perhaps the most important result from our study is identifying the composition of lake ice regimes across different lake-rich arctic landscapes and their susceptibility to future change. Evaluation of lake ice dynamics among study regions suggest that the Barrow Peninsula is most dynamic likely due to depth distributions coupled with proximity to arctic seas and sea ice dynamics that impact winter climatology. The Seward Peninsula, the most southerly region but also susceptible to ocean-affects, also had many intermittent lakes despite overall high proportions of Stable FI lakes. The Kuparuk region is dominated by Stable BI lakes and thus most susceptible to future changes in climate and likely changes in land and water use.

Remote sensing of lake ice regimes with C-band SAR is a useful tool to monitor the effect of shifting lake ice regimes on permafrost, since lake ice regimes can be used as a proxy for thawing of sub-lake permafrost, considered by the Global Climate Observing System as an Essential Climate Variable (ECV). Continued winter warming and variable snow conditions in the Arctic are expected to force changes in lake ice regimes and associated processes and resources. Overall our analysis provides a solid baseline for diverse regions of Arctic Alaska that can be used to evaluate landscape permafrost dynamics, energy balance, regional winter water availability, and freshwater habitats in these and other lake-rich arctic regions.

Acknowledgments

Funding for this study was provided primarily by the National Science Foundation (ARC-1417300) with additional funding and support from the National Parks Service's Inventory and Monitoring Program (P13AC01025), the Arctic Landscape Conservation Cooperative (F13AC00646), and the Bureau of Land Management's Arctic Office (L12AC20023), and the U.S. Geological Survey (GX.18.WB50.E2N01.00). None of the funding sources had any role in the study design, nor in the collection, analysis and interpretation of the data, nor in the writing and submission of the manuscript for publication. We thank Guido Grosse, Richard Beck, Ben Gaglioti, Allen Bondurant, Andy Parsekian, and Ned Rozell for assistance in collecting field ice thickness measurements. We thank ESA for providing ASAR data and SNAP tool suite, with particular thanks to help from the user service desk during their data migration. We thank ASF for providing ERS-1/2, RADARSAT-1, and Sentinel 1A data, and MapReady tool suite. Any use of trade, product, or firm names is for descriptive purposes only and does not imply endorsement by the U.S. Government.

Appendix A. Glossary for abbreviations

ACPnA Arctic Coastal Plain of northern Alaska
ASF Alaska Satellite Facility
BI bedfast ice
DAAC a NASA distributed active archive center
ECV Essential Climate Variable
ERS-1 European Remote Sensing Satellite 1
ERS-2 European Remote Sensing Satellite 2
FI Floating ice
HH horizontal orientation of wave for both transmission and

reception of radar signal

INT lake ice regime that oscillates between bedfast and floating yet shows no trend over time.

MIT maximum ice thickness

NPR-A National Petroleum Reserve – Alaska

NSP northern Seward Peninsula

PDF probability density function

SAR synthetic aperture radar

SLC Single Look Complex data format

Stable BI classified as a bedfast ice lake (> 95% bedfast ice pixels) for 90% or more of the years studied

Stable FI classified as a floating ice lake for 90% or more of the years studied

TRANS-BI lake that transitioned from a floating to a bedfast ice regime

TRANS-FI lake that transitioned from a bedfast to a floating ice regime

References

Ajadi, O.A., Meyer, F.J., Webley, P.W., 2016. Change detection in synthetic aperture radar images using a multiscale-driven approach. Remote Sens. 8 (6), 482. http://dx.doi.org/10.3390/rs8060482.

Alexeev, V.A., Arp, C.D., Jones, B.M., Cai, L., 2016. Arctic sea ice decline contributes to thinning lake ice trend in northern Alaska. Environ. Res. Lett. 11 (7), 074022. http://dx.doi.org/10.1088/1748-9326/11/7/074022.

Arp, C.D., Jones, B.M., Grosse, G., Bondurant, A.C., Romanovsky, V.E., Hinkel, K.M., Parsekian, A.D., 2016. Threshold sensitivity of shallow Arctic lakes and sub-lake permafrost to changing winter climate. Geophys. Res. Lett. http://dx.doi.org/10.1002/2016GL068506.

Arp, C.D., Jones, B.M., Liljedahl, A.K., Hinkel, K.M., Welker, J.A., 2015. Depth, ice thickness, and ice-out timing cause divergent hydrologic responses among Arctic lakes. Water Resour. Res. 51 (12), 9379–9401. http://dx.doi.org/10.1002/2015WR017362.

Arp, C.D., Jones, B.M., Lu, Z., Whitman, M.S., 2012. Shifting balance of lake ice regimes on the Arctic Coastal Plain of northern Alaska. Geophys. Res. Lett. 39, L16503. http://dx.doi.org/10.1029/2012gl052518.

Arp, C.D., Jones, B.M., Urban, F.E., Grosse, G., 2011. Hydrogeomorphic processes of thermokarst lakes with grounded-ice and floating-ice regimes on the Arctic coastal plain, Alaska. Hydrol. Process. 25 (15), 17. http://dx.doi.org/10.1002/hyp.8019.

Atwood, D.K., Gunn, G.E., Roussi, C., Wu, J., Duguay, C., Sarabandi, K., 2015. Microwave backscatter from Arctic lake ice and polarimetric implications. IEEE Trans. Geosci. Remote Sens. 53 (11), 5972–5982. http://dx.doi.org/10.1109/TGRS.2015.2429917.

Bartsch, A., Pointner, G., Leibman, M.O., Dvornikov, Y.A., Khomutov, A.V., Trofaier, A.M., 2017. Circumpolar mapping of ground-fast lake ice. Front. Earth Sci. 5, 12. http://dx.doi.org/10.3389/feart.2017.00012.

Black, R.F., Barksdale, W.L., 1949. Oriented lakes of northern Alaska. The J. Geol. 57 (2), 105–118. http://dx.doi.org/10.1086/625590.

Bojinski, S., Verstraete, M., Peterson, T.C., Richter, C., Simmons, A., Zemp, M., 2014. The concept of essential climate variables in support of climate research, applications, and policy. Bull. Am. Meteorol. Soc. 95 (9), 1431–1443. http://dx.doi.org/10.1175/BAMS-D-13-00047.1.

Bowling, L.C., Kane, D.L., Gieck, R.E., Hinzman, L.D., Lettenmaier, D.P., 2003. The role of surface storage in a low-gradient Arctic watershed. Water Resour. Res. 39 (4), 1087. http://dx.doi.org/10.1029/2002WR001466.

Brewer, M.C., 1958. The thermal regime of an arctic lake. Trans. Am. Geophys. Union 39, 278–284. http://dx.doi.org/10.1029/TR039i002p00278.

Brown, R.S., Duguay, C.R., Mueller, R.P., Moulton, L.L., Doucette, P.J., Tagestad, J.D., 2010. Use of Synthetic Aperture Radar (SAR) to identify and characterize over-wintering areas of fish in ice-covered Arctic rivers: a demonstration with broad whitefish and their habitats in the Sagavanirktok River, Alaska. Trans. Am. Fish. Soc. 139 (6), 1711–1722. http://dx.doi.org/10.1577/T09-176.1.

Burn, C.R., 2002. Tundra lakes and permafrost, Richards Island, western Arctic coast, Canada. Can. J. Earth Sci. 39 (8), 1281–1298. http://dx.doi.org/10.1139/e02-035.

Carson, C.E., Hussey, K.M., 1962. The oriented lakes of Arctic Alaska. The J. Geol. 70, 417–439. http://dx.doi.org/10.1086/626834.

Carter, L.D., 1981. A pleistocene sand sea on the Alaskan Arctic coastal plain. Science 211 (4480), 381–383. http://dx.doi.org/10.1126/science.211.4480.381.

Darbon, J., Cunha, A., Chan, T.F., Osher, S., Jensen, G.J., 2008. Fast nonlocal filtering applied to electron cryomicroscopy. In: Proceedings of the 5th IEEE International Symposium on Biomedical Imaging: From Nano to Macro (ISBI 2008), Paris, France, 14–17 Maypp. 1331–1334. http://dx.doi.org/10.1109/ISBI.2008.4541250.

Dekker, R.J., 1998. Speckle filtering in satellite SAR change detection imagery. Int. J. Remote Sens. 19 (6), 1133–1146. http://dx.doi.org/10.1080/014311698215649.

Duguay, C.R., Bernier, M., Gauthier, Y., Kouraev, A., 2015. Remote sensing of lake and river ice. In: Tedesco, M. (Ed.), Remote Sensing of the Cryosphere. John Wiley & Sons, Ltd., pp. 273–306. http://dx.doi.org/10.1002/9781118368909.ch12.

Duguay, C.R., Flato, G.M., Jeffries, M.O., Menard, P., Morris, K., Rouse, W.R., 2003. Ice-cover variability on shallow lakes at high latitudes: model simulations and observations. Hydrol. Process. 17, 3465–3483. http://dx.doi.org/10.1002/hyp.1394.

Duguay, C.R., Pultz, T.J., Lafleur, P.M., Drai, D., 2002. RADARSAT backscatter characteristics of ice growing on shallow sub-Arctic lakes, Churchill, Manitoba, Canada. Hydrol. Process. 16, 1631–1644. http://dx.doi.org/10.1002/hyp.1026.

Engram, M., 2018. Floating and bedfast lake ice regimes across Arctic Alaska using space-borne SAR imagery from 1992-2016. In: National Science Foundation Arctic Data Center, http://dx.doi.org/10.18739/A2FC5W.

Engram, M., Anthony, K.W., Meyer, F.J., Grosse, G., 2012. Synthetic aperture radar (SAR) backscatter response from methane ebullition bubbles trapped by thermokarst lake ice. Can. J. Remote. Sens. 38 (06), 667–682. http://dx.doi.org/10.5589/m12-054.

Engram, M., Anthony, K.W., Meyer, F.J., Grosse, G., 2013. Characterization of L-band synthetic aperture radar (SAR) backscatter from floating and grounded thermokarst lake ice in Arctic Alaska. Cryosphere 7 (6), 1741–1752. http://dx.doi.org/10.5194/tc-7-1741-2013.

Farquharson, L., Anthony, K.W., Bigelow, N., Edwards, M., Grosse, G., 2016. Facies analysis of yedoma thermokarst lakes on the northern Seward Peninsula, Alaska. Sediment. Geol. 340, 25–37. http://dx.doi.org/10.1016/j.sedgeo.2016.01.002.

French, N., Savage, S., Shuchman, R., Edson, R., Payne, J., Josberger, E., 2004. Remote sensing of frozen lakes on the North Slope of Alaska. In: Paper presented at the Geoscience and Remote Sensing Symposium, 2004. IGARSS '04. Proceedings. 2004 IEEE International, 20–24 Sept. 2004.

Grosse, G., Jones, B., Arp, C., 2013. Thermokarst lake, drainage, and drained basins. In: Shroder, J., Giardino, R., Harbor, J. (Eds.), Treatise on Geomorphology. Academic Press, San Diego, CA, pp. 1–29. http://dx.doi.org/10.1016/B978-0-12-374739-6.00216-5.

Grunblatt, J., Atwood, D., 2014. Mapping lakes for winter liquid water availability using SAR on the North Slope of Alaska. Int. J. Appl. Earth Obs. Geoinf. 27, 63–69. http://dx.doi.org/10.1016/j.jag.2013.05.006. (Part A, (0)).

Gunn, G.E., Brogioni, M., Duguay, C., Macelloni, G., Kasurak, A., King, J., 2015. Observation and modeling of X- and Ku-band backscatter of snow-covered freshwater lake ice. IEEE Journal of Selected Topics in Applied Earth Observations and Remote Sensing 8 (7), 3629–3642. http://dx.doi.org/10.1109/JSTARS.2015.2420411.

Gunn, G.E., Duguay, C.R., Atwood, D.K., King, J., Toose, P., 2018. Observing scattering mechanisms of bubbled freshwater lake ice using polarimetric RADARSAT-2 (C-Band) and UW-Scat (X- and Ku-Bands). IEEE Trans. Geosci. Remote Sens. 1–17.

Hall, D.K., Fagre, D.B., Klasner, F., Linebaugh, G., Liston, G.E., 1994. Analysis of ERS-1synthetic-aperture-radar data of frozen lakes in northern Montana and implications for climate studies. J. Geophys. Res. Oceans 99, 22473–22482.

Heim, K., Wipfli, M., Whitman, M., Arp, C., Adams, J., Falke, J., 2015. Seasonal cues of Arctic grayling movement in a small Arctic stream: the importance of surface water connectivity. Environ. Biol. Fish 1–17. http://dx.doi.org/10.1007/s10641-015-0453-x.

Hinkel, K.M., Frohn, R.C., Nelson, F.E., Eisner, W.R., Beck, R.A., 2005. Morphometric and spatial analysis of thaw lakes and drained thaw lake basins in the western Arctic Coastal Plain, Alaska. Permafr. Periglac. Process. 16 (4), 327–341. http://dx.doi.org/10.1002/ppp.532.

Hopkins, D.M., 1949. Thaw lakes and thaw sinks in the Imuruk Lake area, Seward Peninsula, Alaska. J. Geol. 57, 119–131. http://dx.doi.org/10.1086/625591.

Hopkins, D.M., 1988. The Espenberg maars: a record of explosive volcanic activity in the Devil Mountain-Cape Espenberg area, Seward Peninsula, Alaska. In: Schaaf, J.M. (Ed.), The Bering Sea Land Bridge National Preserve: An Archeological Survey. National Park Service, Alaska Regional Office, pp. 262–321.

Hopkins, D.M., Karlstrom, T.N.V., Black, R., Pewe, R.L., Fernald, A.T., Muller, E.H., 1955. Permafrost and ground water in Alaska. U.S. Geol. Surv. Prof. Pap. 264, 70.

Jeffries, M.O., Morris, K., Liston, G.E., 1996. A method to determine lake depth and water availability on the north slope of Alaska with spaceborne imaging radar and numerical ice growth modelling. Arctic 49 (4), 367–374.

Jeffries, M.O., Morris, K., Weeks, W.F., Wakabayashi, H., 1994. Structural and stratigraphic features and ERS-1 synthetic-aperture radar backscatter characteristics of ice growing on shallow lakes in NW Alaska, winterw1991–1992. J. Geophys. Res. Oceans 99, 22459–22471.

Jones, B.M., Arp, C.D., Hinkel, K.M., Beck, R.A., Schmutz, J.A., Winston, B., 2009. Arctic lake physical processes and regimes with implications for winter water availability and management in the National Petroleum Reserve Alaska. Environ. Manag. 43 (6), 1071–1084. http://dx.doi.org/10.1007/s00267-008-9241-0.

Jones, B.M., Grosse, G., 2013. In: Cooperative, A.L.C. (Ed.), Western Arctic Coastal Plain, Lakes and Drainage Gradients. Arctic Landscape Conservation Cooperative. http://arcticlcc.org/projects/geophysical/thermokarst-lake-drainage/.

Jones, B.M., Grosse, G., Arp, C.D., Jones, M.C., Anthony, K.M.W., Romanovsky, V.E., 2011. Modern thermokarst lake dynamics in the continuous permafrost zone, northern Seward Peninsula, Alaska. J. Geophys. Res. Biogeosci. 116, G00M03. http://dx.doi.org/10.1029/2011jg001666.

Jones, M.C., Grosse, G., Jones, B.M., Anthony, K.W., 2012. Peat accumulation in drained thermokarst lake basins in continuous, ice-rich permafrost, northern Seward Peninsula, Alaska. J. Geophys. Res. Biogeosci. 117http://dx.doi.org/10.1029/2011jg001766. (G00m07).

Jones, B.M., Gusmeroli, A., Arp, C.D., Strozzi, T., Grosse, G., Gaglioti, B.V., Whitman, M.S., 2013. Classification of freshwater ice conditions on the Alaskan Arctic Coastal Plain using ground penetrating radar and TerraSAR-X satellite data. Int. J. Remote Sens. 34 (23), 8267–8279. http://dx.doi.org/10.1080/2150704x.2013.834392.

Jones, B.M., et al., 2017. A lake cover classification to guide research and inform management decisions in an arctic watershed in northern Alaska experiencing climate and land-use change. Ambio. http://dx.doi.org/10.1007/s13280-017-0915-9.

Jorgenson, M.T., Shur, Y., 2007. Evolution of lakes and basins in northern Alaska and discussion of the thaw lake cycle. J. Geophys. Res. Earth Surf. 112 (F2), F02s17. http://dx.doi.org/10.1029/2006jf000531.

Jorgenson, T., Yoshikawa, K., Kanevskiy, M., Shur, Y., Romanovsky, V.E., Marchenko, S.,

Grosse, G., Brown, J., Jones, B.M., 2008. Permafrost characteristics of Alaska. In: Ninth International Conference on Permafrost at University of Alaska Fairbanks (p. Permfrost map of Alaska): Ninth International Conference on Permafrost at University of Alaska Fairbanks, . http://alaska.portal.gina.alaska.edu/catalogs/233-permafrost-characteristics-of-alaska-2008-sha.

Kozlenko, N., Jeffries, M.O., 2000. Bathymetric mapping of shallow water in thaw lakes on the North Slope of Alaska with spaceborne imaging radar. Arctic 53 (3), 306–316.

Lee, J.-S., 1981. Speckle analysis and smoothing of synthetic aperture radar images. Computer Graphics and Image Processing 17 (1), 24–32. http://dx.doi.org/10.1016/S0146-664X(81)80005-6.

Lehner, B., Dőll, P., 2004. Development and validation of a global database of lakes, reservoirs and wetlands. J. Hydrol. 296 (1–4), 1–22. http://dx.doi.org/10.1016/j.jhydrol.2004.03.028.

Leppi, J., Arp, C., Whitman, M., 2015. Predicting late winter dissolved oxygen levels in Arctic lakes using morphology and landscape metrics. Environ. Manag. 1–11. http://dx.doi.org/10.1007/s00267-015-0622-x.

Mellor, J., 1982. Bathymetry of Alaskan Arctic Lakes: A Key to Resource Inventory with Remote Sensing Methods. Dissertation. Institute of Marine Science, University of Alaska Fairbanks.

Mellor, J.C., 1987. A statistical analysis and summary of radar-interpreted Arctic lake depths: an addendum to 12 map products. In: Bur. of Land Manage. Alaska, Anchorage. In Technical Report #11pp. 33.

Mercier, G., Girard-Ardhuin, F., 2006. Partially supervised oil-slick detection by SAR imagery using kernel expansion. IEEE Trans. Geosci. Remote Sens. 44, 2839–2846. http://dx.doi.org/10.1109/TGRS.2006.881078.

Morris, K., Jeffries, M.O., Weeks, W.R., 1995. Ice processes and growth history on Arctic and sub-arctic lakes using ERS-1 SAR data. Polar Record 31, 115–128.

Parsekian, A.D., Jones, B.M., Jones, M., Grosse, G., Walter Anthony, K.M., Slater, L., 2011. Expansion rate and geometry of floating vegetation mats on the margins of thermokarst lakes, northern Seward peninsula, Alaska, USA. Earth Surf. Process. Landf. 36, 1889–1897. http://dx.doi.org/10.1002/esp.2210.

Regmi, P., Grosse, G., Jones, M.C., Jones, B.M., Anthony, K.W., 2012. Characterizing post-drainage succession in Thermokarst Lake Basins on the Seward Peninsula, Alaska with TerraSAR-X backscatter and landsat-based NDVI data. Remote Sens. 4, 3741–3765. http://dx.doi.org/10.3390/rs4123741.

Sellmann, P.V., Brown, J., Lewellen, R.I., McKim, H., Merry, C., 1975. The Classification and Geomorphic Implications of Thaw Lakes on the Arctic Coastal Plain, AlaskaRep. US Army Cold Regions Research and Engineering Laboratory, Hanover, NH, pp. 24.

Sellmann, P.V., Weeks, W.F., Campbell, W.J., 1975. Use of side-looking airborne radar to determine lake depth on the Alaskan North Slope. In: Laboratory, U.S.A.C.R.R.A.E. (Ed.), Special Report No. 230. Cold Regions Research and Engineering Laboratory, Hanover, New Hampshire, pp. 14.

Smith, L.C., Sheng, Y.W., MacDonald, G.M., 2007. A first pan-Arctic assessment of the influence of glaciation, permafrost, topography and peatlands on northern hemisphere lake distribution. Permafr. Periglac. Process. 18 (2), 201–208. http://dx.doi.org/10.1002/ppp.581.

Streever, B., 2002. Science and emotion, on ice: the role of science on Alaska's North Slope. Bioscience 52, 179–184. http://dx.doi.org/10.1641/0006-3568(2002)052[0179:SAEOIT]2.0.CO;2.

Surdu, C.M., Duguay, C.R., Brown, L.C., Prieto, D.F., 2014. Response of ice cover on shallow lakes of the North Slope of Alaska to contemporary climate conditions (1950–2011): radar remote-sensing and numerical modeling data analysis. Cryosphere 8 (1), 167–180. http://dx.doi.org/10.5194/tc-8-167-2014.

Trofaier, A.M., Westermann, S., Bartsch, A., 2017. Progress in space-borne studies of permafrost for climate science: towards a multi-ECV approach. Remote Sens. Environ. http://dx.doi.org/10.1016/j.rse.2017.05.021.

Walter, K.M., Zimov, S.A., Chanton, J.P., Verbyla, D., Chapin, F.S., 2006. Methane bubbling from Siberian thaw lakes as a positive feedback to climate warming. Nature 443 (7107), 71–75. http://dx.doi.org/10.1038/nature05040.

Weeks, W.F., Fountain, A.G., Bryan, M.L., Elachi, C., 1978. Differences in radar return from ice-covered north slope lakes. J. Geophys. Res. 83, 4069–4073.

Weeks, W.F., Gow, A.J., Schertler, R.J., 1981. Ground-truth observation of ice-covered North Slope lakes imaged by radar. In: Laboratory, U.S.A.C.O.E.C.R.R.A.E. (Ed.), Report 81-19. U.S. Army Corps of Engineers Cold Regions research and Engineering Laboratory, Hanover, New Hampshire, pp. 17.

Weeks, W.F., Sellmann, P., Campbell, W.J., 1977. Interesting features of radar imagery of ice covered north slope lakes. J. Glaciol. 18, 129–136.

Wendler, G., Moore, B., Galloway, K., 2014. Strong temperature increase and shrinking sea ice in Arctic Alaska. The Open Atmospheric Science Journal 8, 7–15. http://dx.doi.org/10.2174/1874282301408010007.

White, D.M., Prokein, P., Chambers, M., Lilly, M.R., Toniolo, H., 2008. Use of synthetic aperture radar for selecting Alaskan lakes for winter water use. J. Am. Water Resour. Assoc. 44 (2), 276–284. http://dx.doi.org/10.1111/j.1752-1688.2007.00160.x.

Zhang, T., Jeffries, M.O., 2000. Modeling interdecadal variations of lake-ice thickness and sensitivity to climatic change in northernmost Alaska. Ann. Glaciol. 31, 339–347. http://dx.doi.org/10.1080/10889379909377670.